response to antigenic stimulation and the resultant induction of apoptosis and cell cycle arrest.

Additional ablation of E2F1 attenuates the defects of p57-deficient T cells

Our results indicated that E2F activity is increased in both immature and mature T cells by ablation of p57. To examine whether the defects of p57-deficient T cells are indeed attributable to this activation of E2F, we crossed Lck-Cre/$p57^{[+]/F}$ mice with $E2f1^{-/-}$ mice to generate animals that lack both p57 and E2F1 in T cells. The decreases in the size of the thymus and the number of thymocytes in Lck-Cre/$p57^{[+]/F}$ mice were partially reversed by additional ablation of E2F1 (Figure 4A-B). Flow cytometric analysis showed that E2F1 ablation also resulted in a partial rescue of the increase in the frequency of DN3 cells in Lck-Cre/$p57^{[+]/F}$ mice (Figure 4C-D). This attenuation of the differentiation block at the DN3-DN4 transition led to a partial recovery of the absolute cell numbers of each thymocyte compartment in the p57/E2F1 double-mutant mice (Figure 4E).

In comparison with the partial rescue of defects apparent in p57-deficient thymocytes, additional E2F1 ablation almost completely reversed those in p57-deficient splenic T cells. The number of TCRβ-positive cells in the spleen of Lck-Cre/$p57^{[+]/F}$ mice was thus restored to almost the same level as that of control animals by E2F1 ablation (Figure 4F). In addition, E2F1 deficiency completely reversed the changes in the extent of mitogen-induced BrdU incorporation and apoptosis in splenic T cells from Lck-Cre/$p57^{[+]/F}$ mice compared with those from control mice (Figure 4G-H). These results thus indicated that activation of the E2F pathway indeed contributes to the phenotypes of both p57-deficient immature and mature T cells and that the dependency of these phenotypes on such activation is greater in mature T cells than in immature T cells.

Additional ablation of p53 attenuates the phenotypes of p57 deficiency in immature but not mature T cells

Excessive activation of E2F was previously shown to induce p53-dependent or p53-independent apoptosis in a manner dependent on cellular context.[10-13] Indeed, the abundance of mRNAs for p21, Noxa, and Bax, all of which are downstream targets of p53, was increased in DN3 cells of Lck-Cre/$p57^{[+]/F}$ mice (Figure 5A). Furthermore, the abundance of all 3 mRNAs in DN3 cells of Lck-Cre/$p57^{[+]/F}$/$E2f1^{-/-}$ mice was reduced compared with that for DN3 cells of Lck-Cre/$p57^{[+]/F}$ mice (Figure 5A), although this reversal of p53 activation by E2F1 ablation was only partial. We therefore next crossed Lck-Cre/$p57^{[+]/F}$ mice with $p53^{-/-}$ mice to generate animals that lack both p57 and p53 in T cells. The size of the thymus in Lck-Cre/$p57^{[+]/F}$/$p53^{-/-}$ mice was indistinguishable from that in control mice, and we did not detect an increase in the frequency of DN3 cells in the double-mutant animals (Figure 5B-D). The cell numbers for each thymocyte subset in Lck-Cre/$p57^{[+]/F}$ mice were also completely recovered by additional p53 ablation; in particular, the number of ISP cells in Lck-Cre/$p57^{[+]/F}$/$p53^{-/-}$ mice exceeded that in controls (Figure 5E). Collectively, these results suggested that the differentiation block at the DN3-DN4 transition induced by p57 loss is attributable to hyperactivation of p53.

We next examined whether p53 hyperactivation is also responsible for the defects of p57-deficient mature T cells. Whereas the decrease in the number of TCRβ-positive cells in the spleen of Lck-Cre/$p57^{[+]/F}$ mice was completely reversed by the additional ablation of E2F1 (Figure 4F), the ablation of p53 did not reproduce this effect (Figure 6A). Consistent with this result, the abundance of mRNAs for p53 target genes, including those for p21, Noxa, and Bax, was not increased in splenic T cells of Lck-Cre/$p57^{[+]/F}$ mice compared with those of control animals in the absence or presence of anti-CD3ε stimulation (Figure 6B). We also measured BrdU incorporation and the frequency of apoptosis after mitogenic stimulation, and found that additional depletion of p53 did not affect the phenotypes of p57-deficient splenic T cells (Figure 6C-D). Together, these results suggested that, in contrast to immature T cells, the induction of apoptosis and cell cycle arrest by p57 loss in mature T cells are p53 independent.

Given that activated E2F1 was previously shown to increase transcription of the caspase-8 and Bid genes, as well as to enhance Fas signaling in mature T cells,[26] such effects might underlie the increased level of apoptosis in p57-deficient mature T cells. We therefore measured the abundance of mRNAs for caspase-8 and Bid in splenic $CD3^+$ T cells from Lck-Cre/$p57^{[+]/+}$ and Lck-Cre/$p57^{[+]/F}$ mice with or without anti-CD3ε stimulation. We found that the amounts of these mRNAs were indeed increased in $CD3^+$ T cells of Lck-Cre/$p57^{[+]/F}$ mice compared with the control cells after anti-CD3ε stimulation (Figure 6E), suggesting that the caspase-8–Bid pathway contributes to the phenotypes of p57-deficient mature T cells.

Loss of p57 predisposes immature T cells to thymic lymphoma

Given that our data suggested that p53 suppresses aberrant expansion of p57-deficient immature T cells, we examined whether the simultaneous loss of p57 and p53 might eventually result in tumorigenesis. At 8 weeks of age, some of Lck-Cre/$p57^{[+]/F}$/$p53^{-/-}$ mice indeed developed aggressive lymphomas characterized by massive thymic enlargement (Figure 7A). In Figure 7A, 1 of the fastest developing lymphomas in Lck-Cre/$p57^{[+]/F}$/$p53^{-/-}$ mice is shown. Flow cytometric analysis showed a marked increase in the size of the ISP cell population in the Lck-Cre/$p57^{[+]/F}$/$p53^{-/-}$ mice (Figure 7B-C). All of the double-mutant mice died between 14 and 24 weeks of age, indicating that the lymphomas were fatal. Comparison of the timing of thymic lymphoma development demonstrated that the p57/p53 double-mutant mice developed this condition with a reduced latency compared with $p53^{-/-}$ mice, and that Lck-Cre/$p57^{[+]/F}$/$p53^{+/-}$ mice also exhibited a markedly reduced viability compared with $p53^{+/-}$ mice (Figure 7D). None of 13 Lck-Cre/$p57^{[+]/F}$ mice developed lymphoma for up to 500 days of age, supporting the notion that p53 suppresses aberrant expansion of p57-deficient T cells. We thus concluded that p57 and p53 cooperatively prevent excessive proliferation of T cells in the thymus and that disruption of this p57-p53 axis results in lymphomagenesis.

Discussion

Previous studies have indicated that the differentiation of DN3 cells into DN4 cells depends on the balance between p53 activity and pre-TCR signaling (Figure 7E upper left).[4-6] Mice deficient in RAG1/2, DNA-PK, or CD3γ thus exhibit a differentiation block at the DN3 to DN4 stages that is attributable to impaired formation of the pre-TCR complex and consequent abrogation of pre-TCR signaling (Figure 7E upper center). On the other hand, mice deficient in p53 often develop lymphoma,[27] supporting the notion that p53 activity is required for appropriate T-cell development (Figure 7E upper right). We have

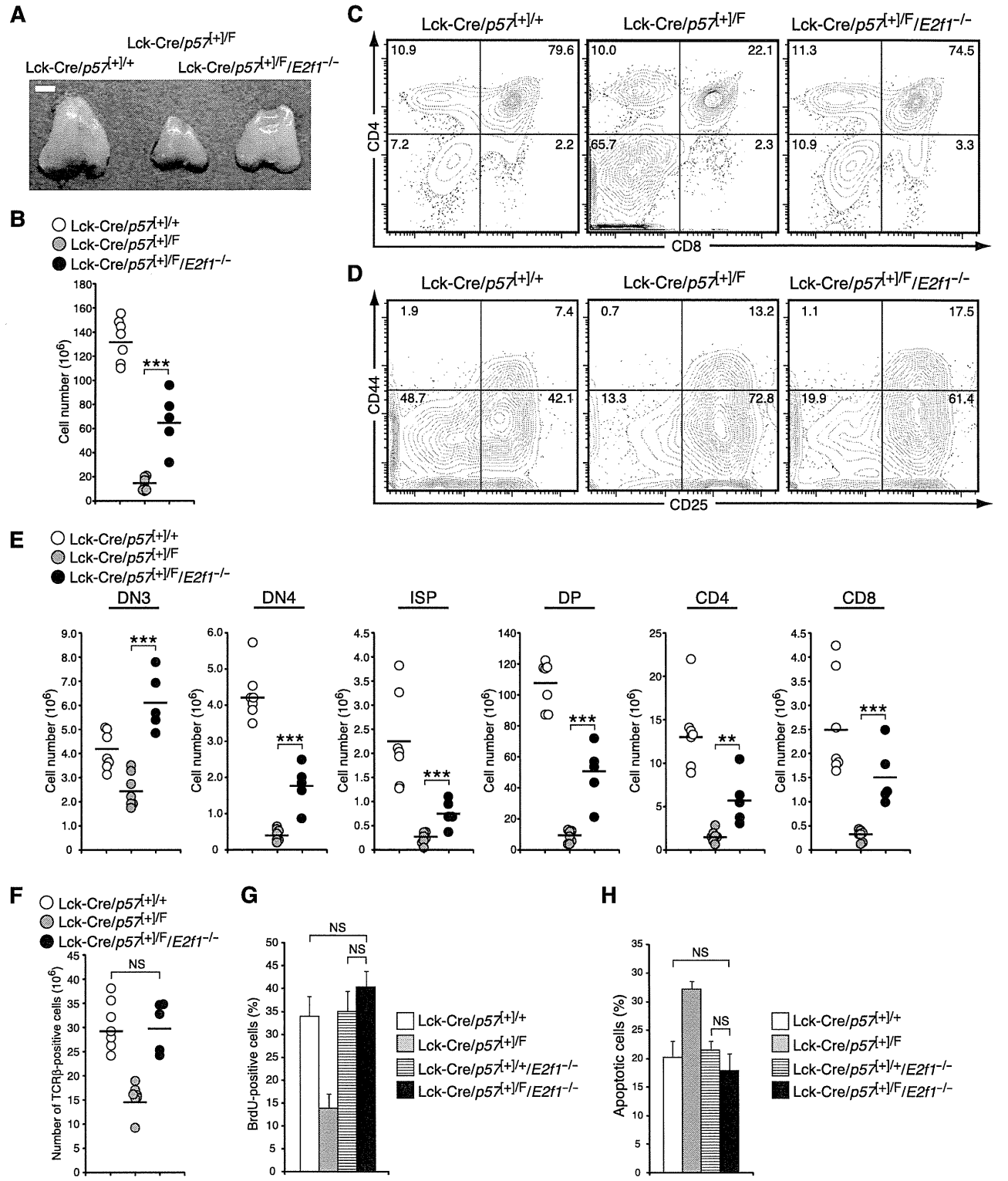

Figure 4. Additional ablation of E2F1 attenuates the defects of immature and mature T cells in p57-deficient mice. (A) Gross appearance of the thymus of Lck-Cre/$p57^{[+]/+}$, Lck-Cre/$p57^{[+]/F}$, and Lck-Cre/$p57^{[+]/F}$/$E2f1^{-/-}$ mice at 8 weeks of age. Scale bar, 2 mm. (B) Total number of thymocytes for individual Lck-Cre/$p57^{[+]/+}$ (n = 7), Lck-Cre/$p57^{[+]/F}$ (n = 7), and Lck-Cre/$p57^{[+]/F}$/$E2f1^{-/-}$ (n = 5) mice at 8 weeks of age. ***$P < .005$. (C-D) Representative flow cytometric analysis of CD4 vs CD8 on thymocytes (C) as well as of CD44 vs CD25 on electronically gated lineage-negative DN thymocytes (D) from Lck-Cre/$p57^{[+]/+}$, Lck-Cre/$p57^{[+]/F}$, and Lck-Cre/$p57^{[+]/F}$/$E2f1^{-/-}$ mice at 8 weeks of age. Percentages of each fraction are indicated. (E) Absolute cell number for thymocyte subsets from individual Lck-Cre/$p57^{[+]/+}$ (n = 7), Lck-Cre/$p57^{[+]/F}$ (n = 7), and Lck-Cre/$p57^{[+]/F}$/$E2f1^{-/-}$ (n = 5) mice at 8 weeks of age determined by flow cytometry. **$P < .01$, ***$P < .005$. (F) Number of TCRβ-positive cells among splenocytes from individual Lck-Cre/$p57^{[+]/+}$ (n = 7), Lck-Cre/$p57^{[+]/F}$ (n = 7), and Lck-Cre/$p57^{[+]/F}$/$E2f1^{-/-}$ (n = 5) mice at 8 weeks of age. (G-H) Splenic $CD3^+$ T cells from mice of the indicated genotypes at 8 weeks of age were stimulated with anti-CD3ε (5 μg/mL) for 36 hours and exposed to BrdU during the final 1 hour of incubation. They were then stained with anti-BrdU and propidium iodide, and the percentages of BrdU-positive cells (G) and of sub-G_1 (apoptotic) cells (H) were determined by flow cytometry. Data are means ± SD for 3 mice.

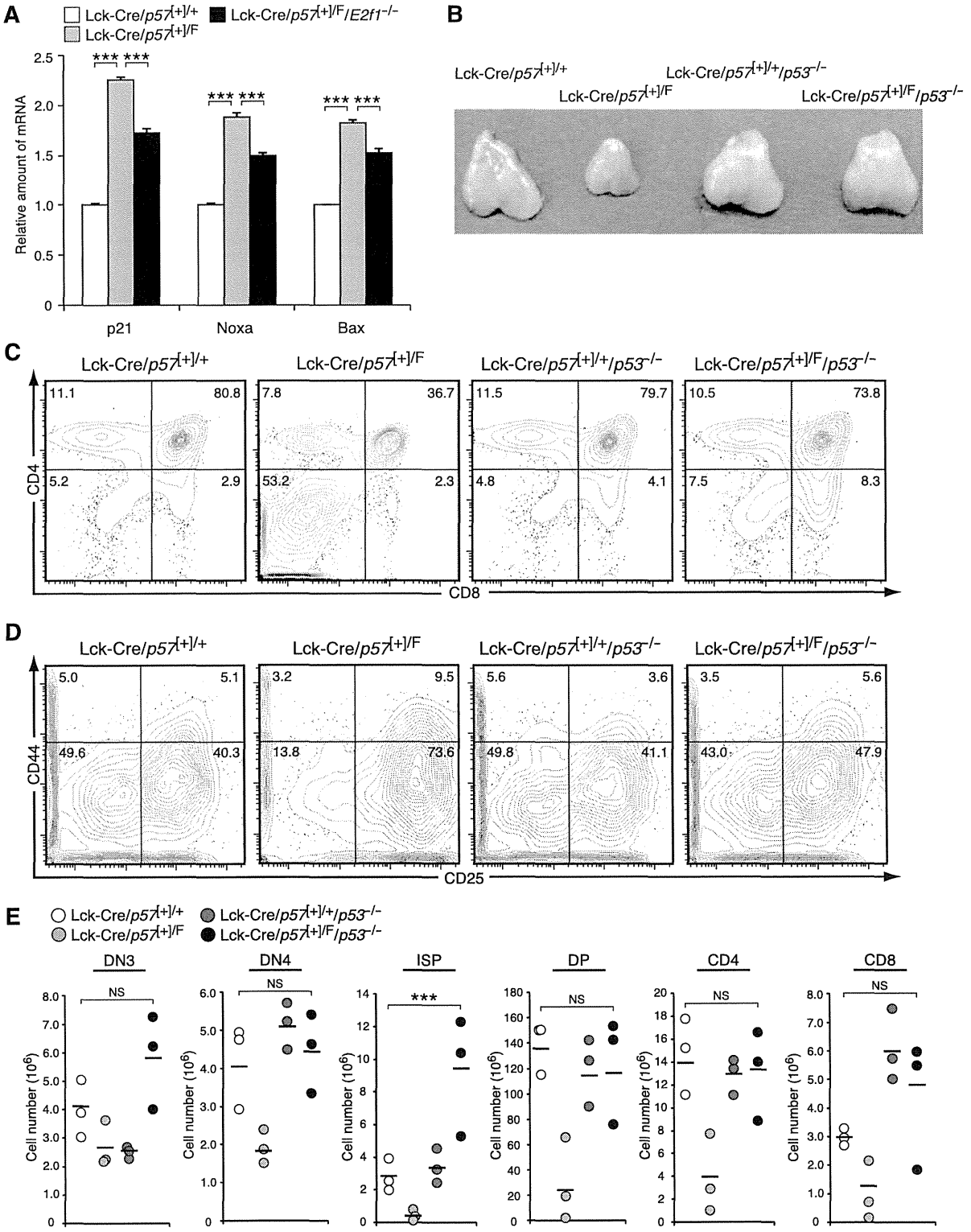

Figure 5. The pre-T cell differentiation block in p57-deficient mice is overcome by additional ablation of p53. (A) RT and real-time PCR analysis of p21, Noxa, and Bax mRNAs in DN3 thymocytes from Lck-Cre/$p57^{[+]/+}$, Lck-Cre/$p57^{[+]/F}$, and Lck-Cre/$p57^{[+]/F}$/$E2f1^{-/-}$ mice at 8 weeks of age. Normalized data are expressed relative to the corresponding value for control mice and are means ± SD for 3 mice. ***$P < .005$. (B) Gross appearance of the thymus of Lck-Cre/$p57^{[+]/+}$, Lck-Cre/$p57^{[+]/F}$, Lck-Cre/$p57^{[+]/+}$/$p53^{-/-}$, and Lck-Cre/$p57^{[+]/F}$/$p53^{-/-}$ mice at 7 weeks of age. Scale bar, 2 mm. (C-D) Representative flow cytometric analysis of CD4 vs CD8 on thymocytes (C) as well as of CD44 vs CD25 on electronically gated lineage-negative DN thymocytes (D) from Lck-Cre/$p57^{[+]/+}$, Lck-Cre/$p57^{[+]/F}$, Lck-Cre/$p57^{[+]/+}$/$p53^{-/-}$, and Lck-Cre/$p57^{[+]/F}$/$p53^{-/-}$ mice at 7 weeks of age. Percentages of each fraction are indicated. (E) Absolute cell numbers determined by flow cytometry for thymocyte subsets from individual Lck-Cre/$p57^{[+]/+}$, Lck-Cre/$p57^{[+]/F}$, Lck-Cre/$p57^{[+]/+}$/$p53^{-/-}$, and Lck-Cre/$p57^{[+]/F}$/$p53^{-/-}$ mice at 7 weeks of age ($n = 3$). ***$P < .005$.

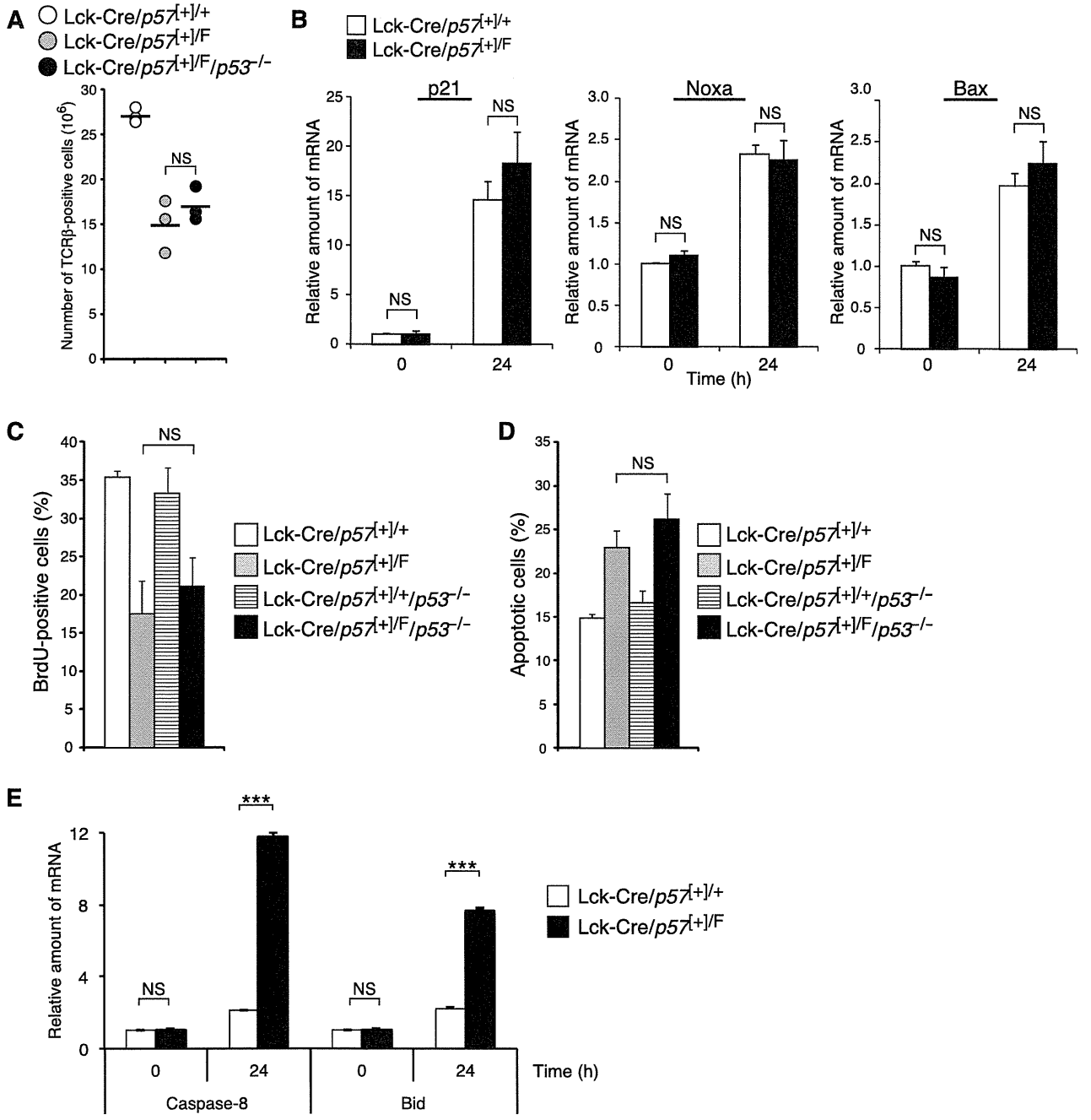

Figure 6. The proliferation and survival defects of mature T cells from p57-deficient mice are not rescued by additional ablation of p53. (A) Number of TCRβ-positive cells among splenocytes from individual Lck-Cre/$p57^{[+]/+}$, Lck-Cre/$p57^{[+]/F}$, and Lck-Cre/$p57^{[+]/F}/p53^{-/-}$ mice at 7 weeks of age (n = 3). (B) Splenic $CD3^+$ T cells from Lck-Cre/$p57^{[+]/+}$ and Lck-Cre/$p57^{[+]/F}$ mice at 8 weeks of age were stimulated with anti-CD3ε (5 μg/mL) for the indicated times, after which the abundance of p21, Noxa, and Bax mRNAs was determined by RT and real-time PCR analysis. Normalized data are expressed relative to the corresponding value for cells from control mice at time 0 and are means ± SD for 3 mice. (C-D) Splenic $CD3^+$ T cells from Lck-Cre/$p57^{[+]/+}$, Lck-Cre/$p57^{[+]/F}$, Lck-Cre/$p57^{[+]/+}/p53^{-/-}$, and Lck-Cre/$p57^{[+]/F}/p53^{-/-}$ mice at 7 weeks of age were stimulated with anti-CD3ε for 36 hours and exposed to BrdU during the final 1 hour of incubation. They were then stained with anti-BrdU and propidium iodide, and the percentages of BrdU-positive cells (C) and of sub-G_1 (apoptotic) cells (D) were determined by flow cytometry. Data are means ± SD for 3 mice. (E) Splenic $CD3^+$ T cells from Lck-Cre/$p57^{[+]/+}$ and Lck-Cre/$p57^{[+]/F}$ mice at 8 weeks of age were stimulated as in panel B, after which the abundance of caspase-8 and Bid mRNAs was determined by RT and real-time PCR analysis. Normalized data are expressed relative to the corresponding value for cells from control mice at time 0 and are means ± SD for 3 mice. ***$P < .005$.

now shown that ablation of p57 induces p53 hyperactivation as a result of upregulation of E2F activity in thymocytes. Whereas genomic rearrangement at the TCRβ locus and intracellular expression of TCRβ in p57-deficient DN3 cells were indistinguishable from those in control cells, the abundance of pTα mRNA was increased in the p57-deficient DN3 cells, suggesting that the extent of pre-TCR signaling was also increased in these cells (Figure 7E lower left). However, p53 hyperactivation dominates this increased level of pre-TCR signaling, leading to a differentiation block at the DN3-DN4 transition.

Whereas additional ablation of E2F1 completely rescued the phenotypes of p57-deficient splenic T cells, the reversal of those of

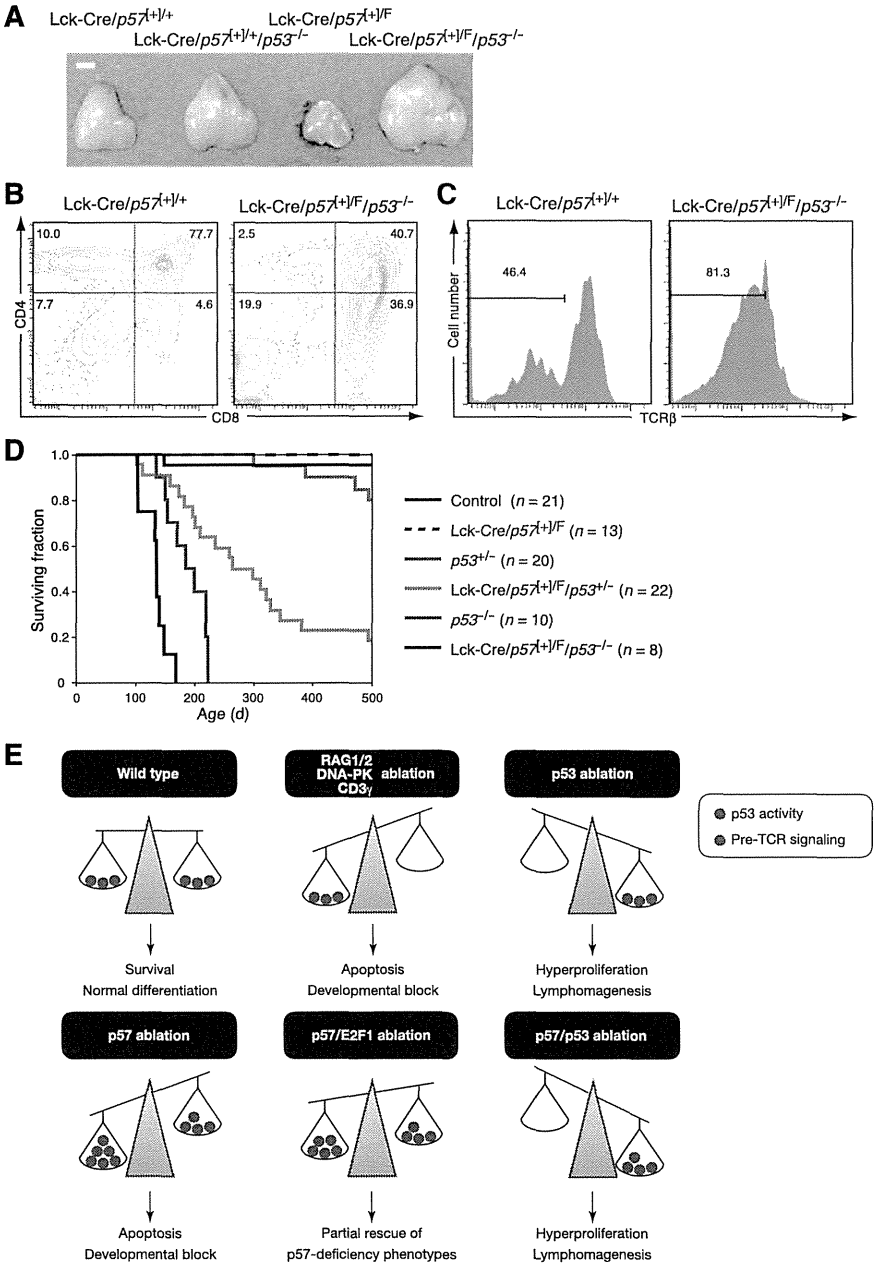

Figure 7. Mice lacking both p57 and p53 develop lymphoma. (A) Gross appearance of the thymus of Lck-Cre/$p57^{[+]/+}$, Lck-Cre/$p57^{[+]/+}/p53^{-/-}$, Lck-Cre/$p57^{[+]/F}$, and Lck-Cre/$p57^{[+]/F}/p53^{-/-}$ mice at 8 weeks of age. Scale bar, 2 mm. (B-C) Representative flow cytometric analysis of CD4 vs CD8 on thymocytes (B) as well as of TCRβ on electronically gated CD8 SP cells (C) from Lck-Cre/$p57^{[+]/+}$ and Lck-Cre/$p57^{[+]/F}/p53^{-/-}$ mice shown in panel A. Percentages of each fraction are indicated. (D) Kaplan-Meier plot for overall survival of mice of the indicated genotypes. (E) Model for the role of p57 in T cell differentiation and prevention of lymphomagenesis. Differentiation of pre-T cells depends on a balance between p53 activity and pre-TCR signaling. Ablation of p57 results in hyperactivation of p53 and thereby induces apoptosis in and blocks the development of immature T cells. Additional ablation of E2F1 results in a partial rescue of the phenotypes associated with p57 deficiency. The simultaneous ablation of p57 and p53 results in aberrant expansion of immature T cells, eventually leading to the development of fatal thymic lymphoma. See Discussion for further details.

p57-deficient immature T cells by E2F1 ablation was partial (Figure 7E lower center). Given that previous studies indicate that other members of the E2F family, such as E2F2 or E2F3, also contribute to the maturation of immature T cells,[28] activation of these other family members might be involved in the phenotypes of p57-deficient immature T cells.

Activated E2F promotes cell cycle progression by increasing the transcription of genes that contribute to the G_1-S transition.[8] E2F also promotes transcription of apoptosis-related genes, including those for ATM and ASPP1 that induce apoptosis through activation of p53.[29,30] Consistent with these findings, we found that the amounts of ATM and ASPP1 mRNAs as well as those of mRNAs derived from p53 target genes were increased in p57-deficient immature T cells in association with an increase in the frequency of apoptosis (Figure 7E lower left). Furthermore, additional ablation of p53 rescued p57-deficiency phenotypes in immature T cells, suggesting that the reduction in the number of these cells elicited by p57 ablation is attributable to p53-dependent cell cycle arrest and induction of apoptosis. Our data show that the predominant response to p53 activation in p57-deficient immature T cells is cell cycle arrest, although the mechanism by which a cell selects cell cycle arrest or apoptosis as the appropriate response to p53 activation remains elusive.

We found that the number of ISP cells in CD4-Cre/$p57^{[+]/F}$ mice and Lck-Cre/$p57^{[+]/F}/p53^{-/-}$ mice is even greater than that in corresponding control mice (Figures 3E and 5E), suggesting that loss of p57 may promote E2F-driven cell proliferation in ISP cells to a greater extent than in other T-cell fractions. Consistent with this notion, p57/p53 double-mutant mice eventually develop fatal thymic lymphomas characterized by accumulation of ISP cells (Figure 7E lower right). Ablation of p57 alone did not confer an increased susceptibility to lymphoma development, suggesting that p53 suppresses

such development in the context of p57 deficiency. In conclusion, our study has unveiled the physiological importance of the p57-E2F-p53 pathway in the proper development of T cells as well as in the prevention of lymphomagenesis, with our results providing the basis for a new paradigm in the relation between CDK inhibitors, development of the immune system, and lymphomagenesis.

Acknowledgments

The authors thank C. B. Wilson for CD4-Cre mice, L. Yamasaki for *E2f1*$^{-/-}$ mice, A. Niihara, C. Mitai, and M. Tanaka for technical assistance, and members of our laboratory for comments on the manuscript.

Authorship

Contribution: A.M. and S.T. performed experiments and wrote the manuscript; and K.I.N. designed research, interpreted data, and wrote the manuscript.

Conflict-of-interest disclosure: The authors declare no competing financial interests.

The current affiliation for A.M. is the Cancer Genetics Program, Beth Israel Deaconess Cancer Center, Departments of Medicine and Pathology, Beth Israel Deaconess Medical Center, Harvard Medical School, Boston, MA 02215.

Correspondence: Keiichi I. Nakayama, Department of Molecular and Cellular Biology, Medical Institute of Bioregulation, Kyushu University, 3-1-1 Maidashi, Higashi-ku, Fukuoka, Fukuoka 812-8582, Japan; e-mail: nakayak1@bioreg.kyushu-u.ac.jp.

References

1. Hosoya T, Maillard I, Engel JD. From the cradle to the grave: activities of GATA-3 throughout T-cell development and differentiation. *Immunol Rev.* 2010;238(1):110-125.
2. Naito T, Tanaka H, Naoe Y, Taniuchi I. Transcriptional control of T-cell development. *Int Immunol.* 2011;23(11):661-668.
3. Jameson SC, Bevan MJ. T-cell selection. *Curr Opin Immunol.* 1998;10(2):214-219.
4. Haks MC, Krimpenfort P, van den Brakel JH, Kruisbeek AM. Pre-TCR signaling and inactivation of p53 induces crucial cell survival pathways in pre-T cells. *Immunity.* 1999;11(1):91-101.
5. Jiang D, Lenardo MJ, Zúñiga-Pflücker JC. p53 prevents maturation to the CD4+CD8+ stage of thymocyte differentiation in the absence of T cell receptor rearrangement. *J Exp Med.* 1996;183(4):1923-1928.
6. Guidos CJ, Williams CJ, Grandal I, Knowles G, Huang MT, Danska JS. V(D)J recombination activates a p53-dependent DNA damage checkpoint in scid lymphocyte precursors. *Genes Dev.* 1996;10(16):2038-2054.
7. Sherr CJ, Roberts JM. Living with or without cyclins and cyclin-dependent kinases. *Genes Dev.* 2004;18(22):2699-2711.
8. Burkhart DL, Sage J. Cellular mechanisms of tumour suppression by the retinoblastoma gene. *Nat Rev Cancer.* 2008;8(9):671-682.
9. Polager S, Ginsberg D. p53 and E2f: partners in life and death. *Nat Rev Cancer.* 2009;9(10):738-748.
10. DeGregori J, Leone G, Miron A, Jakoi L, Nevins JR. Distinct roles for E2F proteins in cell growth control and apoptosis. *Proc Natl Acad Sci U S A.* 1997;94(14):7245-7250.
11. Kowalik TF, DeGregori J, Schwarz JK, Nevins JR. E2F1 overexpression in quiescent fibroblasts leads to induction of cellular DNA synthesis and apoptosis. *J Virol.* 1995;69(4):2491-2500.
12. Phillips AC, Bates S, Ryan KM, Helin K, Vousden KH. Induction of DNA synthesis and apoptosis are separable functions of E2F-1. *Genes Dev.* 1997;11(14):1853-1863.
13. Qin XQ, Livingston DM, Kaelin WG Jr, Adams PD. Deregulated transcription factor E2F-1 expression leads to S-phase entry and p53-mediated apoptosis. *Proc Natl Acad Sci U S A.* 1994;91(23):10918-10922.
14. Sherr CJ, Roberts JM. CDK inhibitors: positive and negative regulators of G1-phase progression. *Genes Dev.* 1999;13(12):1501-1512.
15. Deng C, Zhang P, Harper JW, Elledge SJ, Leder P. Mice lacking p21$^{CIP1/WAF1}$ undergo normal development, but are defective in G1 checkpoint control. *Cell.* 1995;82(4):675-684.
16. Nakayama K, Ishida N, Shirane M, et al. Mice lacking p27^{Kip1} display increased body size, multiple organ hyperplasia, retinal dysplasia, and pituitary tumors. *Cell.* 1996;85(5):707-720.
17. Fero ML, Rivkin M, Tasch M, et al. A syndrome of multiorgan hyperplasia with features of gigantism, tumorigenesis, and female sterility in p27^{Kip1}-deficient mice. *Cell.* 1996;85(5):733-744.
18. Kiyokawa H, Kineman RD, Manova-Todorova KO, et al. Enhanced growth of mice lacking the cyclin-dependent kinase inhibitor function of p27^{Kip1}. *Cell.* 1996;85(5):721-732.
19. Takahashi K, Nakayama K, Nakayama KI. Mice lacking a CDK inhibitor, p57^{Kip2}, exhibit skeletal abnormalities and growth retardation. *J Biochem.* 2000;127(1):73-83.
20. Zhang P, Liégeois NJ, Wong C, et al. Altered cell differentiation and proliferation in mice lacking p57^{KIP2} indicates a role in Beckwith-Wiedemann syndrome. *Nature.* 1997;387(6629):151-158.
21. Matsumoto A, Takeishi S, Kanie T, et al. p57 is required for quiescence and maintenance of adult hematopoietic stem cells. *Cell Stem Cell.* 2011;9(3):262-271.
22. Wolfer A, Bakker T, Wilson A, et al. Inactivation of Notch 1 in immature thymocytes does not perturb CD4 or CD8T cell development. *Nat Immunol.* 2001;2(3):235-241.
23. Wolfer A, Wilson A, Nemir M, MacDonald HR, Radtke F. Inactivation of Notch1 impairs VDJbeta rearrangement and allows pre-TCR-independent survival of early alpha beta Lineage Thymocytes. *Immunity.* 2002;16(6):869-879.
24. Matsuoka S, Edwards MC, Bai C, et al. p57^{KIP2}, a structurally distinct member of the p21^{CIP1} Cdk inhibitor family, is a candidate tumor suppressor gene. *Genes Dev.* 1995;9(6):650-662.
25. Laurent J, Bosco N, Marche PN, Ceredig R. New insights into the proliferation and differentiation of early mouse thymocytes. *Int Immunol.* 2004;16(8):1069-1080.
26. Cao Q, Xia Y, Azadniv M, Crispe IN. The E2F-1 transcription factor promotes caspase-8 and bid expression, and enhances Fas signaling in T cells. *J Immunol.* 2004;173(2):1111-1117.
27. Pant V, Quintás-Cardama A, Lozano G. The p53 pathway in hematopoiesis: lessons from mouse models, implications for humans. *Blood.* 2012;120(26):5118-5127.
28. DeGregori J. The genetics of the E2F family of transcription factors: shared functions and unique roles. *Biochim Biophys Acta.* 2002;1602(2):131-150.
29. Berkovich E, Ginsberg D. ATM is a target for positive regulation by E2F-1. *Oncogene.* 2003;22(2):161-167.
30. Fogal V, Kartasheva NN, Trigiante G, et al. ASPP1 and ASPP2 are new transcriptional targets of E2F. *Cell Death Differ.* 2005;12(4):369-376.

Tyk2-Dependent Bystander Activation of Conventional and Nonconventional Th1 Cell Subsets Contributes to Innate Host Defense against *Listeria monocytogenes* Infection

Tomomitsu Hashiguchi,*,† Akiko Oyamada,† Koji Sakuraba,*,† Kazuya Shimoda,‡ Keiichi I. Nakayama,† Yukihide Iwamoto,§ Yasunobu Yoshikai,* and Hisakata Yamada*

IL-12, which is produced in response to intracellular bacteria, such as *Listeria monocytogenes*, promotes the development of pathogen-specific Th1 cells that play an important role in host defense. However, it has also been known that CD44^{high} memory-phenotype CD4 T cells with Th1 functions naturally occur in naive mice, and that lymphopenia-induced proliferation of naive CD4 T cells generates memory-phenotype CD4 T cells with Th1 functions, although their differentiation mechanism and contribution to host defense are unclear. In this study, we analyzed the development and the functions of the different subsets of Th1 cells by using mice lacking tyrosine kinase 2 (Tyk2), a member of the Janus kinase family critically involved in IL-12 signaling. In contrast with the case of conventional Ag-specific Th1 cells, the development of naturally occurring Th1 cells was not impaired in Tyk2-deficient mice. In addition, Th1 cells were normally generated from Tyk2-deficient naive CD4 T cells via lymphopenia-induced proliferation. Nevertheless, all these Th1 subsets, including conventional Ag-induced Th1 cells, produced IFN-γ in response to IL-12 in a Tyk2-dependent manner. Importantly, such Tyk2-dependent bystander IFN-γ production of any Th1 subsets conferred early protection against *L. monocytogenes* infection. Thus, Tyk2-mediated IL-12 signaling is differentially required for the development of different Th1 cell subsets but similarly induces their bystander IFN-γ production, which contributes to innate host defense against infection with intracellular bacteria. *The Journal of Immunology*, **2014, 192: 4739–4747.**

The induction of pathogen-specific CD4 and CD8 T cells that produce IFN-γ is critical for the elimination of intracellular bacteria, such as *Listeria monocytogenes* (1). However, because clonal expansion and functional differentiation of Ag-specific T cells, that is, adaptive immune response, require several days, Ag-nonspecific innate IFN-γ production plays a role at an early phase of *L. monocytogenes* infection. A variety of IFN-γ–producing lymphocytes, including NK cells, NK-T cells, and γδ T cells, are involved in innate host defense against *L. monocytogenes* infection (2–4). It is also known that CD8 T cells that express memory markers confer innate protection against *L. monocytogenes* infection (5).

Such memory phenotype (MP) CD8 T cells can be found in naive mice, even in Tec kinase–deficient mice, which lack naive conventional CD8 T cells (6–8). Therefore, the naturally occurring MP CD8 T cells are thought to belong to a lineage distinct from conventional CD8 T cells and are also called innate-like CD8 T cells (9). In fact, MP CD8 T cells in naive mice produced IFN-γ in response to IL-12, which was enhanced by an addition of IL-18 (10, 11). They were also activated during *L. monocytogenes* infection and conferred significant protection (5, 8, 12, 13). In addition to the naturally occurring MP CD8 T cells, MP CD8 T cells in naive mice might also include CD8 T cells that have acquired MP and effector functions after lymphopenia-induced proliferation (LIP) (14) and bona-fide memory CD8 T cells specific for self- or environmental Ags. Interestingly, it was demonstrated that effector CD8 T cells specific for an unrelated Ag, for example, OVA, produced IFN-γ during listerial infection and contributed to host defense (5). Thus, even Ag-induced CD8 T cells can be involved in both innate and adaptive immune responses.

MP CD4 T cells, a portion of which are functionally Th1 cells, are also found in naive mice (15–17), but their functions are less known compared with MP CD8 T cells. Similar to MP CD8 T cells, such naturally occurring Th1 cells developed in the absence of Tec kinases, and were activated and produced IFN-γ in response to IL-12 in vitro or during *L. monocytogenes* infection in vivo (15). However, in vivo relevance of the bystander activation of Th1 cells in innate host defense remains unclear. It is also unknown whether LIP-induced MP CD4 T cells, a portion of which is functionally Th1 type (18), as well as conventional Ag-induced Th1 cells exert bystander IFN-γ production.

Tyrosine kinase 2 (Tyk2), a member of the Janus kinase family, is involved in various cytokine signalings and is particularly important for transducing signals from IL-12Rβ1 chain, the common subunit for IL-12Rs and IL-23Rs (19). Hence IL-12–induced IFN-γ production by NK cells was diminished in the absence of Tyk2 (20). Tyk2-deficient mice failed to mount Ag-specific Th1 responses after immunization or infection (21, 22), supporting the importance of IL-12 signaling in the differentiation of Th1 cells. However, interestingly, we have found that differentiation of

*Division of Host Defense, Medical Institute of Bioregulation, Kyushu University, Fukuoka 812-8582, Japan; †Department of Orthopedic Surgery, Graduate School of Medical Sciences, Kyushu University, Fukuoka 812-8582, Japan; ‡Department of Gastroenterology and Hematology, Faculty of Medicine, University of Miyazaki, Miyazaki 889-1692, Japan; and §Department of Molecular and Cellular Biology, Medical Institute of Bioregulation, Kyushu University, Fukuoka 812-8582, Japan

Received for publication November 14, 2013. Accepted for publication March 8, 2014.

This work was supported by Grants-in-Aid for Scientific Research, Japan Society for the Promotion of Science, and the Grants for Excellent Graduate Schools, Ministry of Education, Culture, Sports, Science and Technology, Japan.

Address correspondence and reprint requests to Dr. Hisakata Yamada, Division of Host Defense, Medical Institute of Bioregulation, Kyushu University, 3-1-1 Maidashi Higashi-ku, Fukuoka 812-8582, Japan. E-mail address: hisakata@bioreg.kyushu-u.ac.jp

Abbreviations used in this article: KO, knockout; LIP, lymphopenia-induced proliferation; LN, lymph node; MP, memory phenotype; Tyk2, tyrosine kinase 2; WT, wild-type.

www.jimmunol.org/cgi/doi/10.4049/jimmunol.1303067

IFN-γ–producing effector CD8 T cells did not require Tyk2 (23). In line with this observation, comparable or even larger numbers of IFN-γ–producing CD8 T cells were detected in IL-12–deficient mice (24, 25). Thus, the requirement of Tyk2-mediated signaling differs among different IFN-γ–producing T cell populations. In this regard, it is of interest to examine whether the Th1 cell subsets that arise in noninfectious conditions, namely, naturally occurring Th1 cells and LIP-generated Th1 cells, are dependent on Tyk2 signaling. In addition, Tyk2-deficient mice would be useful for evaluating the importance of IL-12–induced bystander activation of Th1 cells in vivo.

In this study, we examined the differentiation mechanism and the functions of different Th1 subsets by using Tyk2-deficient mice. We found that nonconventional naturally occurring and LIP-generated Th1 cells did not require Tyk2-mediated signaling for their development, whereas Tyk2-dependent bystander activation of these Th1 cell subsets contributes to the innate protection against *L. monocytogenes* infection.

Materials and Methods

Mice

C57BL/6 mice were purchased from Charles River Breeding Laboratories (Yokohama, Japan). Tyk2 knockout (KO) mice were generated as previously described (21). OT-II (transgenic mice expressing TCR specific for $OVA_{323-339}$ peptide on I-A^b), RAG1 KO, IFN-γ KO, and CD45.1-congenic C57BL/6 mice were obtained from The Jackson Laboratory (Bar Harbor, ME) and were maintained in specific pathogen-free conditions in our institute. Sex- and age-matched mice were used between 6 and 8 wk of age, except for the experiments analyzing neonatal thymus in which 2-d-old mice were used. This study design was approved by the Committee of Ethics on Animal Experiment in Faculty of Medicine (Kyushu University). Experiments were carried out under the control of the Guidelines for Animal Experimentation.

Abs and flow cytometric analysis

Fluorochrome-conjugated mAbs and reagents used for flow cytometric analysis were as follows: FITC-conjugated anti-CD44 (IM-7), anti-CD45.2 (104), anti-TCRδ (GL3), Alexa Fluor 488–conjugated anti–IFN-γ (XMF1.2), PE-conjugated anti–IFN-γ (XMF1.2), anti-CD62L (MEL-14), anti-CD4 (GK1.5), anti-Vα2 (B20.1), allophycocyanin-conjugated anti-CD3 (17A2), anti-CD8 (53.6.7), anti-CD45.1 (A20), anti-CD45.2 (104), PerCP-Cy5.5–conjugated anti-CD4 (CT-CD4), and anti-NK1.1 (PK136) mAbs were purchased from BD Biosciences (San Jose, CA). To detect cytokine production, we cultured cells for 5 h with PMA (25 ng/ml) and ionomycin (1 μg/ml; Sigma-Aldrich, St. Louis, MO) or for 18 h with IL-12 (5 ng/ml; PeproTech, Rocky Hill, NJ) or IL-18 (10 ng/ml; PeproTech), or combination of both. Brefeldin A (10 μg/ml; Sigma-Aldrich) was added to the cultures for the last 4 h. The cell culture medium used in this study was RPMI 1640 (Pure Chemicals) supplemented with 10% FBS (Cell Culture Technologies, Gravesano, Switzerland), 100 U/ml penicillin, 100 mg/ml streptomycin, and 0.5 mM 2-ME. Intracellular staining was performed using BD Cytofix/Cytoperm Kit (BD Biosciences). Stained cells were run on a FACSCalibur flow cytometer (BD Biosciences), and the data were analyzed using BD CellQuest software (BD Biosciences).

Cell purification

Naive CD4 T cells were purified from lymph node (LN) cells in OT-II or wild-type (WT) C57BL/6 mice. Cells were first stained with anti-CD8 (2.43) and anti–I-A/E (M5/114.112.5) mAbs, followed by an incubation with Dynabead sheep anti-rat IgG (Invitrogen, Carlsbad, CA) to negatively select CD4 T cells. Then naive CD4 T cells were purified by using anti-CD62L microbeads and an autoMACS cell separator (Miltenyi Biotec, Bergisch Gladbach, Germany). The purity of $CD44^{low}$ $CD62L^{high}CD4^+$ T cells was >95%. For purifying $CD44^{high}$ and $CD44^{low}$ CD4 T cells, negatively selected CD4 T cells from the spleens and the LNs were stained with FITC-conjugated anti-CD44, PE-conjugated anti-CD4, and allophycocyanin-conjugated anti-CD3 mAbs. $CD44^{high}$ or $CD44^{low}$ $CD3^+$ $CD4^+$ T cells were sorted by FACSAriaII (BD Biosciences). The purity of $CD44^{high}$ or $CD44^{low}$ CD4 T cells was >97%. For the experiments transferring bulk CD4 T cell population, CD4 T cells were directly purified from splenocytes and LN cells by using anti-CD4 microbeads and an autoMACS cell separator (Miltenyi Biotec). The purity of $CD4^+$ T cells was >90%.

In vivo priming of OT-II cells

Naive CD4 T cells purified from WT (CD45.1/1) and Tyk2 KO (CD45.2/2) OT-II mice were mixed (5×10^5 cells/each) and injected i.v. into WT C57BL/6 mice (CD45.1/2). On the next day, the recipient mice were injected s.c. into the base of the tail with an emulsion containing 100 μg OVA and CFA (DIFCO, Detroit, MI). Mice were killed after 1 wk, and splenocytes were used for the analysis.

LIP of CD4 T cells

Naive CD4 T cells purified from WT (CD45.1/1) or Tyk2 KO (CD45.2/2) mice were mixed (1×10^6 cells/each) and injected i.v. into RAG1 KO mice or sublethally irradiated WT (CD45.1/2) mice. After 2 wk, when most of the transferred CD4 T cells had converted to $CD44^{high}$, splenocytes were harvested from the RAG1 KO recipients and used for the in vitro analysis, whereas the irradiated recipients were subjected to the infection experiments.

L. monocytogenes *infection*

Mice were inoculated i.p. with 3×10^5 CFU *L. monocytogenes* strain EGD, which correspond to one tenth of the LD_{50} for WT C57BL/6 mice, in 0.2 ml PBS. Peritoneal cavity was lavaged with 3 ml PBS, whereas the spleens were removed and dispersed in 3 ml PBS to measure bacterial number. Various dilutions of the samples were spread on trypto-soya agar plates (Nissui Pharmaceutical, Tokyo, Japan), and colonies were counted after incubation for 24 h at 37°C. Heat-killed listeria was prepared by incubating viable *L. monocytogenes* at 72°C for 60 min.

Induction of Th1 cells in vitro

LN cells from WT OT-II mice were cultured with 10 ng/ml $OVA_{323-339}$ peptide, 1 ng/ml recombinant mouse IL-12 (PeproTech), and 10 μg/ml anti–IL-4 mAb (11B11) at $5–7 \times 10^5$ cells/well in 48-well plates. At day 4, cells were harvested, washed with PBS, and used for the transfer experiments. Differentiation to Th1 was confirmed by intracellular staining of IFN-γ after stimulation with PMA and ionomycin.

Statistics

Statistical significance was calculated by the two-tailed Mann–Whitney *U* test using Prism software (GraphPad Software). A p value <0.05 was considered statistically significant.

Results

Tyk2-dependent differentiation of Ag-induced Th1 cells from naive CD4 T cells

It has been shown that the induction of Ag-specific Th1 responses was impaired in Tyk2-deficient mice (21, 22, 26). However, because IL-12 could also induce T cell proliferation (21), it is possible that the reduced Th1 responses in Tyk2-deficient mice resulted from an insufficient clonal expansion of Ag-specific CD4 T cells, but not from an impaired differentiation into Th1 cells. To test this possibility, we compared in vivo Th1 differentiation of OVA-specific TCR transgenic CD4 T (OT-II) cells of Tyk2-deficient (KO) and WT mice. Naive WT and KO OT-II cells were cotransferred into CD45-congenic recipient mice, which were subsequently immunized with OVA (Fig. 1A). One week after immunization, Th1 differentiation of donor cells in the spleen was examined by detecting IFN-γ production after stimulation with PMA and ionomycin. We found that, although total number of OT-II cells did not differ, the frequency and the number of IFN-γ–producing cells was much lower in KO than in WT cells (Fig. 1B, 1C). Thus, Tyk2-mediated IL-12 signaling is critical for the differentiation of Ag-induced Th1 cells from naive CD4 T cells.

We then examined whether the Ag-specific Th1 cells generated from WT mice produce IFN-γ in response to IL-12 without antigenic stimulation. The spleen cells harvested in the earlier experiment were stimulated with IL-12 or IL-12 and IL-18 in the presence of brefeldin A. We detected IFN-γ production of WT

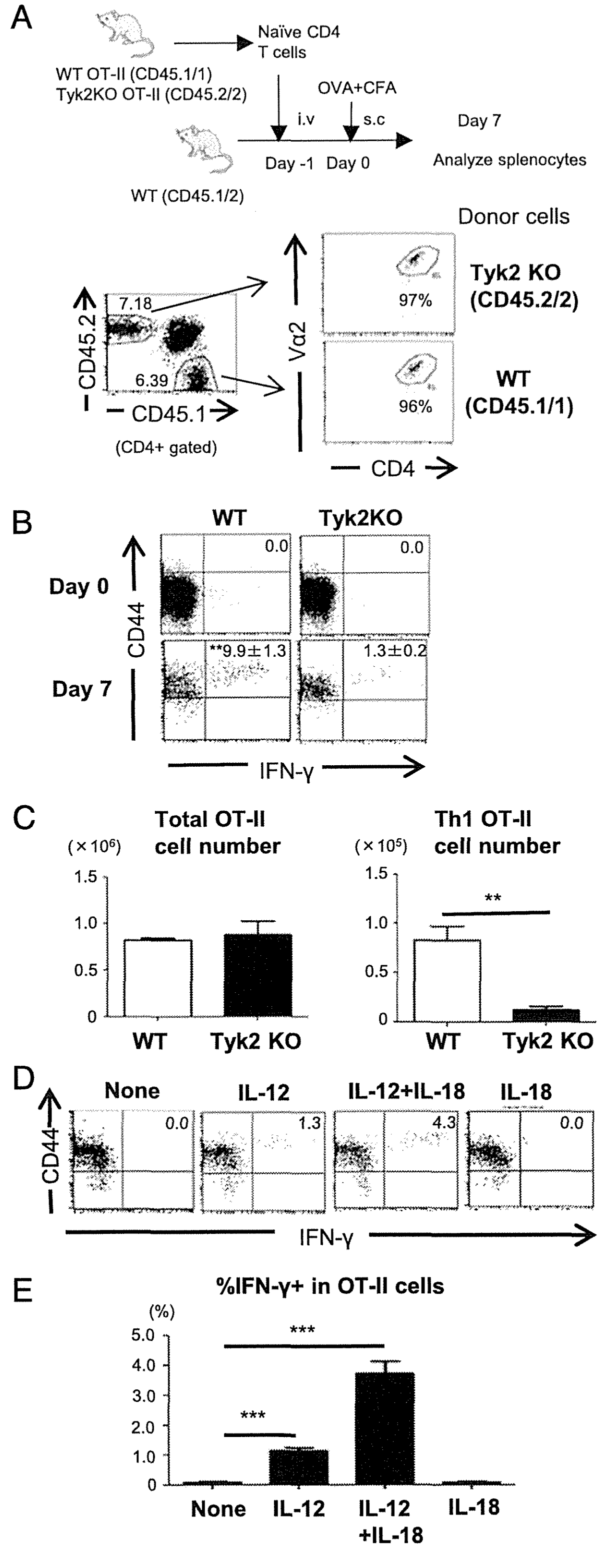

FIGURE 1. Tyk2-dependent differentiation of Ag-induced Th1 cells. (**A**) Naive CD4 T cells from WT (CD45.1/1) and Tyk2 KO (CD45.2/2) OT-II mice were cotransferred i.v. into WT (CD45.1/2) mice ($n = 3$), which were immunized with OVA on the next day. The spleen cells were harvested 1 wk after immunization and were subjected to flow cytometric analysis or were restimulated for functional assays. Lower panels show the expression of OT-II TCR (Vα2) and CD4 in each donor cell population. (**B**) Intracellular staining of IFN-γ after stimulation with PMA and ionomycin on days 0 (before transfer) and 7. Representative dot plots are shown after gating on $CD45.2^-$ (WT) or $CD45.1^-$ (Tyk2 KO) $CD4^+$ T cells. The number in each panel indicates the mean ± SEM percentage of IFN-γ^+ cells in donor OT-II cells. (**C**) The number of total (*left panel*) and IFN-γ–producing (*right panel*) donor OT-II cells in the spleen is shown. Data are mean ± SEM. $^{**}p < 0.01$. (**D**) The splenocytes were stimulated with IL-12, IL-18, or IL-12 and IL-18 for 18 h and were tested for intracellular staining of IFN-γ. Data are shown after gating on $CD45.2^-$ WT OT-II cells. (**E**) Mean percentages of IFN-γ^+ cells in OT-II cells are shown ($n = 3$). Error bars represent SEM. $^{***}p < 0.001$. Data are representative of three independent experiments.

OT-II cells stimulated with IL-12, which was augmented by the addition of IL-18 (Fig. 1D, 1E). Stimulation with IL-18 alone did not induce IFN-γ production. These results indicate that IL-12 signaling induces not only development but also bystander IFN-γ production of Ag-induced Th1 cells.

Tyk2-independent development of naturally occurring Th1 cells in naive mice

We next examined the requirement of Tyk2-mediated signaling for the development of Th1 cells that naturally occur in naive mice. Splenocytes and thymocytes of naive WT or Tyk2 KO C57BL/6 mice were stimulated with PMA and ionomycin to detect Th1 cells. We found comparable numbers of $CD44^{high}$ CD4 T cells in the spleen or the thymus of WT and Tyk2 KO mice (Fig. 2A). There was no difference in the percentage of IFN-γ–producing cells among $CD44^{high}$ CD4 T cells in WT and KO mice (Fig. 2B, 2C). Virtually no $CD44^{low}$ cells produced IFN-γ. Such Th1-type MP CD4 T cells were found even in the neonatal thymus, suggesting their naturally occurring origin (data not shown). Although MP CD4 T cells in both the spleen and the thymus included $NK1.1^+$ cells, there was no difference in the percentage of IFN-γ^+ cells in either $NK1.1^+$ or $NK1.1^-$ CD4 T cell population between WT and KO mice (Fig. 2D, 2E). Thus, NKT cells and naturally occurring Th1 cells in naive mice develop independently of Tyk2.

These data suggest differential requirements of IL-12 signaling for the development of naturally occurring Th1 cells and conventional Ag-induced Th1 cells, but it is also possible that the requirement of Tyk2 for IL-12 signaling differs between these two Th1 cell populations. So, we examined the responsiveness of naturally occurring Th1 cells to IL-12 in vitro. As reported previously (15), stimulation with IL-12 induced IFN-γ production from $CD44^{high}$ CD4 T cells in naive WT mice, which was augmented by the presence of IL-18 (Fig. 2F, 2G). However, Tyk2-deficient $CD44^{high}$ CD4 T cells produced much less IFN-γ in response to IL-12 signaling. Therefore, IL-12 signaling in naturally occurring Th1 cells was actually Tyk2 dependent. This, in turn, indicates that their development is IL-12 independent.

Tyk2-independent differentiation of naive CD4 T cells into Th1 cells by LIP

MP T cells found in the periphery of naive mice might include those that have been generated via LIP, in addition to those that naturally occur in the thymus. In this study, we investigated the involvement of Tyk2 in the differentiation of Th1 cells generated via LIP. Naive Tyk2 KO or WT CD4 T cells were transferred into RAG1 KO mice, and spleen cells were harvested 2 wk later (Fig. 3A). Most of the transferred CD4 T cells from both Tyk2 KO and WT mice converted to express high levels of CD44 in the lymphopenic recipients (Fig. 3B). There was also no difference in the number between Tyk2 KO and WT donor cells (Fig. 3C). By examining cytokine production after stimulation with PMA and ionomycin, we found no difference in the percentage and the number of donor cells producing IFN-γ (Fig. 3B, 3C). Similar results were obtained by using naive OT-II cells as the donor (data not shown). Thus, LIP-induced Th1 cells resemble the naturally occurring Th1 cells

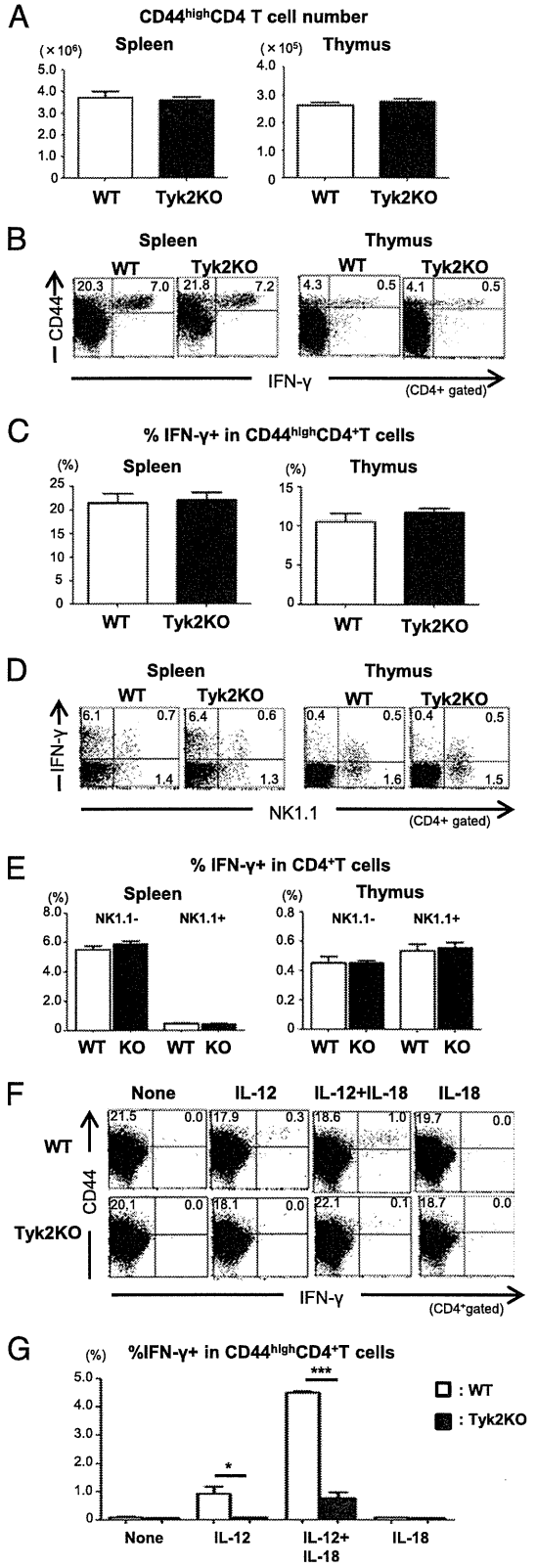

FIGURE 2. Tyk2-independent development of naturally occurring Th1 cells in naive mice. (**A**) The absolute number of $CD44^{high}$ CD4 T cells in the spleen and thymus of naive WT and Tyk2 KO mice was calculated after flow cytometric analysis. Data are mean ± SEM ($n = 3$). (**B**) Splenocytes and thymocytes from naive WT and Tyk2 KO mice were tested for intracellular staining of IFN-γ after stimulation with PMA and ionomycin. Representative dot plots are shown after gating on $CD4^+$ cells. (**C**) The percentages of IFN-γ^+ cells in $CD44^{high}CD4^+$ splenocytes (*left*) or $CD44^{high}CD4^+CD8^-$ thymocytes (*right*) are shown. Data are mean ± SEM. (**D**) Representative dot plots depicting IFN-γ production from $NK1.1^+$ and $NK1.1^-$ $CD4^+$splenocytes or $CD4^+CD8^-$ thymocytes (*right*) after PMA and ionomycin stimulation. Data are shown after gating on $CD4^+$ cells. (**E**) Mean percentages of IFN-γ^+ cells $NK1.1^+$ and $NK1.1^-$ $CD4^+$ splenocytes (*left*) or $CD4^+CD8^-$ thymocytes (*right*) are shown. (**F**) Splenocytes from naive WT or Tyk2 KO mice were stimulated with IL-12, IL-18, or IL-12 and IL-18 for 18 h and were tested for intracellular staining of IFN-γ. Representative dot plots are shown after gating on $CD4^+$ cells. (**G**) Mean percentages of IFN-γ^+ cells in $CD44^{high}$ $CD4^+$ T cells are shown. $*p < 0.05$, $***p < 0.001$. Data are representative of three independent experiments.

in naive mice in that they develop independently of Tyk2. We tested the in vitro response to IL-12 of the LIP-generated Th1 cells and found that only WT donor cells produced IFN-γ in response to IL-12 (Fig. 3D, 3E). Thus, LIP-generated Th1 cells can also produce IFN-γ in a bystander manner and their IL-12 signaling is Tyk2 dependent.

Tyk2-dependent bystander IFN-γ production from naturally occurring Th1 cells confers protection against bacterial infection

Tyk2-deficient mice showed an impaired early protection against *L. monocytogenes* infection (27). Although Tyk2-dependent IFN-γ production by NK cells, NK-T cells, MP CD8 T cells, as well as TCR γδ T cells might be involved in the early protection against listerial infection, earlier results also suggest a role of Th1 cells. We reported that in situ IFN-γ production of CD8 T cells during *L. monocytogenes* infection was detected by staining intracellular IFN-γ after brief culture with brefeldin A (28). By using this technique, we detected IFN-γ production from $CD44^{high}$ CD4 T cells in WT, but not in KO, mice as early as at day 2 after listerial infection (Fig. 4A), suggesting bystander IFN-γ production of naturally occurring Th1 cells. We also found that listerial Ag-specific IFN-γ production, which was detected by adding heat-killed bacteria to the culture, was impaired in Tyk2 KO CD4 T cells at day 7 postinfection (Fig. 4A), indicating that the development of bacterial Ag-specific Th1 cells was also Tyk2 dependent. Bacterial number in the spleen and the peritoneal cavity of Tyk2 KO mice was significantly increased compared with WT mice (Fig. 4B), indicating that the impaired IFN-γ production of KO CD4 T cells was not due to a decreased bacterial burden. The difference in bacterial number between WT and Tyk2 KO mice was smaller compared with our previous study (27), possibly because of the altered bacterial virulence and different number of inoculated bacteria. By examining IFN-γ production of various cell subsets at day 2 postinfection, it was revealed that the majority of IFN-γ–producing cells were NK cells, which were reduced in Tyk2 KO mice (Fig. 4C). Notably, the proportion of CD4 T cells in IFN-γ–producing cells exceeded that of CD8 T cells, NKT cells, or γδ T cells. Most IFN-γ–producing CD4 T cells were $NK1.1^-$ (data not shown).

To verify the relevance of Tyk2-dependent bystander IFN-γ production of naturally occurring Th1 cells in host defense, we transferred CD4 T cell subsets from naive WT mice into Tyk2 KO mice before *L. monocytogenes* infection (Fig. 5A). We found that transferring $CD44^{high}$ CD4 T cells, but not $CD44^{low}$ CD4 T cells, conferred significant protection against listerial infection in Tyk2 KO mice (Fig. 5B). Depleting $NK1.1^+$ cells from the donor CD4 T cells did not affect the degree of protection (data not shown). To confirm that the protection provided by $CD44^{high}$ CD4 T cells was mediated by IFN-γ, we transferred WT or IFN-γ KO CD4 T cells and found that IFN-γ KO CD4 T cells could not reduce bacterial burden in Tyk2 KO mice (Fig. 5C, 5D). There was no difference in the proportion of $CD44^{high}$ cells between WT and IFN-γ KO CD4

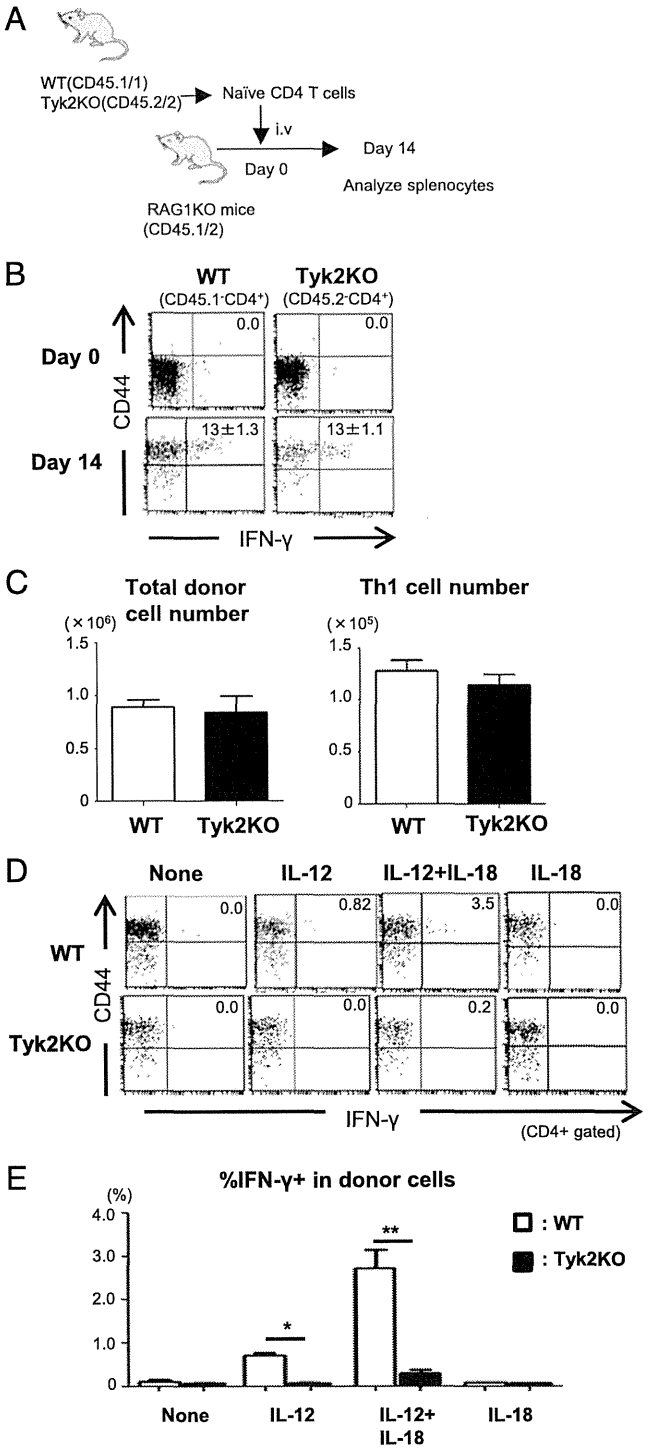

FIGURE 3. Tyk2-independent differentiation of naive CD4 T cells into Th1 cells by LIP. (**A**) Naive CD4 T cells from WT (CD45.1/1) and Tyk2 KO (CD45.2/2) mice were transferred i.v. into RAG1 KO (CD45.1/2) mice (n = 3). Two weeks after transfer, splenocytes were harvested and restimulated before flow cytometric analysis. (**B**) The splenocytes were stained for intracellular IFN-γ after stimulation with PMA and ionomycin. Representative dot plots are shown after gating on $CD4^+CD45.2^-$ (WT) or $CD4^+CD45.1^-$ (Tyk2 KO) cells. The upper panels show donor T cells before transfer. The numbers in the panels are the mean percentages of IFN-γ–producing cells in $CD4^+$ cells. (**C**) Absolute number of total (*left*) and Th1 (*right*) donor CD4 T cells in the spleen is shown. Data are mean ± SEM. (**D**) The splenocytes were stimulated with IL-12, IL-18, and IL-12 + IL-18 for 18 h and were tested for intracellular staining of IFN-γ. Representative dot plots are shown after gating on donor $CD4^+$ cells. (**E**) Mean percentages of IFN-γ–producing cells in donor CD4 T cells are shown. $*p < 0.05$, $**p < 0.01$. Data are representative of three independent experiments.

T cells (data not shown). We also found that CD4 T cells from naive WT, but not Tyk2 KO mice, decreased bacterial burden in IFN-γ KO mice (data not shown). These results suggest that Tyk2-dependent bystander IFN-γ production by naturally occurring Th1 cells is involved in the host defense against listerial infection.

Tyk2-dependent host defense by LIP-induced Th1 cells

To test whether LIP-induced Th1 cells can also confer innate protection against listerial infection, we transferred naive CD4 T cells from WT or Tyk2 KO mice into irradiated IFN-γ KO mice that were infected with *L. monocytogenes* 2 wk later (Fig. 6A). We confirmed that both WT and Tyk2 KO CD4 T cells differentiated into Th1 cells after LIP in the irradiated IFN-γ KO recipients (Fig. 6B). However, only WT CD4 T cells spontaneously produced IFN-γ in response to listerial infection. Furthermore, bacterial number was decreased in mice transferred with WT, but not Tyk2 KO CD4 T cells (Fig. 6C). Thus, LIP-induced Th1 cells can also be involved in host defense against *L. monocytogenes* in a Tyk2-dependent manner.

Bystander IFN-γ production from Ag-induced Th1 cells can be involved in host defense against bacterial infection

Although IL-12–induced bystander IFN-γ production was also detected in conventional Ag-specific Th1 cells (Fig. 1D, 1E), its in vivo relevance remains unclear. To verify this, we transferred WT or Tyk2 KO naive OT-II cells into IFN-γ KO mice that were subsequently immunized with OVA. Then the mice were challenged with *L. monocytogenes* infection, and bacterial number in the peritoneal cavity and the spleen was examined at day 2 (Fig. 7A). We detected IFN-γ production by the transferred WT OT-II cells (data not shown) and also found that transferring WT, but not Tyk2 KO OT-II cells significantly decreased bacterial burden in IFN-γ KO mice (Fig. 7B). By transferring the same number of in vitro–induced Th1 or naive OT-II cells from WT mice into Tyk2 or IFN-γ KO mice before *L. monocytogenes* infection (Fig. 7C), we found that Th1, but not naive WT OT-II cells conferred protection against *L. monocytogenes* infection in both Tyk2 KO mice and IFN-γ KO mice (Fig. 7D, 7E). These results indicate that even conventional Ag-induced Th1 cells can contribute to innate host defense against listerial infection via bystander IFN-γ production.

Discussion

Differentiation of naive CD4 T cells to various Th cell subsets is strongly influenced by the cytokine milieu. It is established that naive CD4 T cells primed in the presence of IL-12 preferentially differentiate into Th1 cells (29). We confirmed by using OT-II cells that the differentiation of Th1 cells was impaired in the absence of Tyk2, an essential molecule for IL-12 signaling. Induction of the bacterial Ag-specific Th1 cells during listerial infection was also reduced in Tyk2 KO mice. These results seem reasonable because immunization with CFA or listerial infection induces IL-12 production from APCs, and thereby provides an environment suitable for Th1 differentiation. However, there are subsets of Th1 cells that develop under noninfectious conditions. These include naturally occurring MP CD4 T cells in naive mice and MP CD4 T cells generated via LIP (18). We demonstrated in this study by using Tyk2-deficient mice that these two Th1 cell subsets differentiated independently of Tyk2-mediated cytokine signaling, including IL-12. They might use alternative cytokines for differentiation, but it is also possible that they do not require any cytokine signals. Interestingly, IL-12– or Tyk2-independent differentiation of naive CD8 T cells to IFN-γ–producing Tc1 cells was also reported (23–25). In addition, we have found that naturally occurring IL-17–

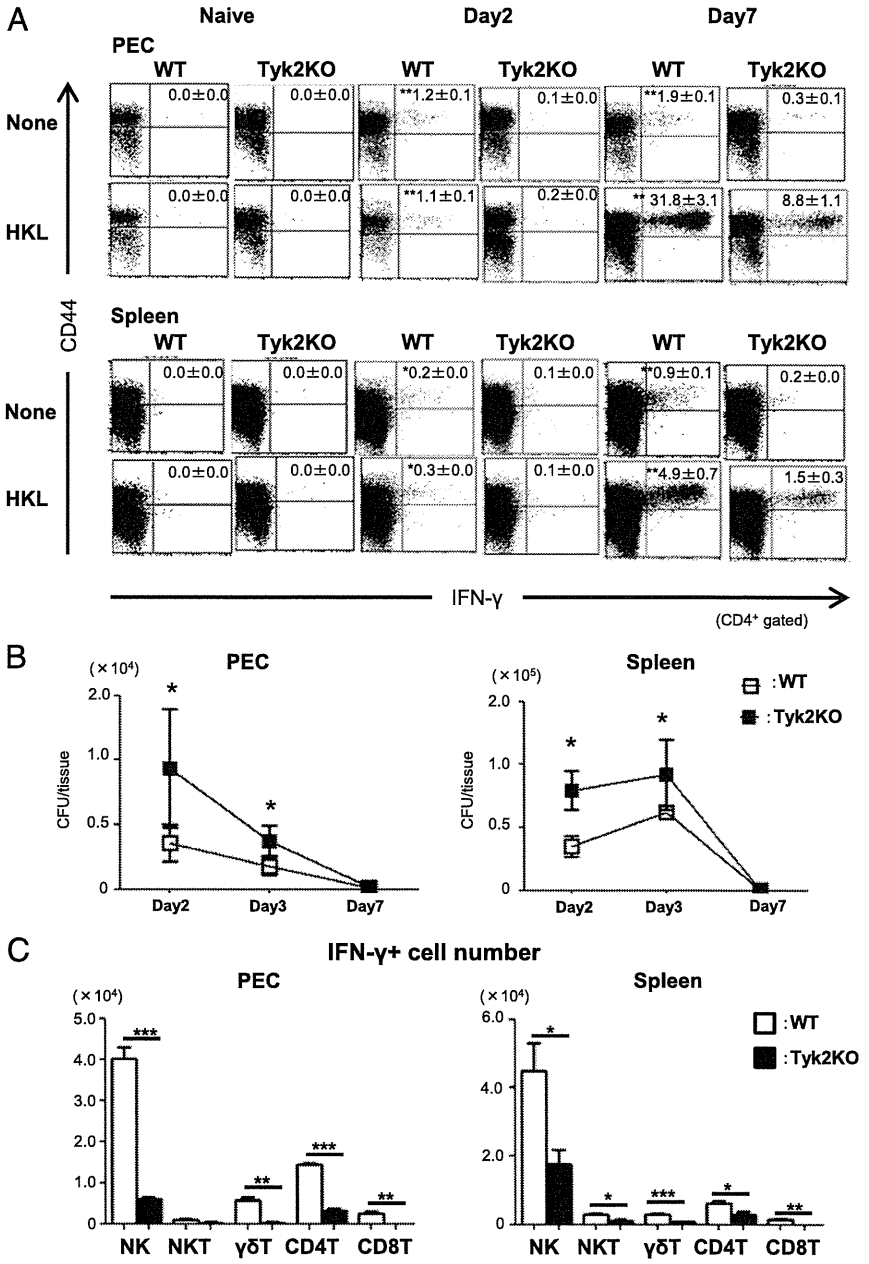

FIGURE 4. Tyk2-dependent bystander IFN-γ production from naturally occurring Th1 cells during bacterial infection. (**A**) Peritoneal exudate cells (PECs) and spleen cells in WT (n = 3) and Tyk2 KO (n = 3) mice were harvested on days 2, 3, and 7 after i.p inoculation with *L. monocytogenes*. Cells were cultured for 5 h with or without stimulation with heat-killed listeria in the presence of brefeldin A and were subjected to intracellular staining of IFN-γ. Representative dot plots are shown after gating on $CD4^+$ cells. The numbers in the panels are the mean percentages of IFN-γ–producing cells in $CD4^+$ cells. (**B**) Bacterial numbers in the peritoneal cavity and the spleen are shown. (**C**) Absolute number of IFN-γ–producing cell population in PECs and spleen of WT (white bars, n = 3) and Tyk2 KO (black bars, n = 3) mice 2 d after *L monocytogenes* infection. Intracellular IFN-γ was detected after 5-h culture with brefeldin A. Data are mean ± SEM. $*p < 0.05$, $**p < 0.01$, $***p < 0.001$. Data are representative of three separate experiments.

producing TCR γδ T cells do not require STAT3, which mediates IL-6 signaling and is critical for Th17 differentiation (30). Thus, there are differences in the requirement for cytokine signaling in the differentiation of effector T cell populations.

The origin of MP CD4 T cells in naive mice, a portion of which are functionally Th1 cells, is unclear. They might include nonconventional naturally occurring Th1 cells differentiated in the thymus (15), Th1 cells generated via LIP (18), as well as conventional memory Th1 cells induced by environmental Ags/pathogens. In this regard, our results provide a clue to understand their origin. Thus, most of these T cells might not be conventional Ag-induced Th1 cells but nonconventional naturally occurring Th1 cells or LIP-induced Th1 cells, because they can develop in the absence of Tyk2. Younes et al. (17) also reported that MP CD4 T cells in naive mice are distinct from Ag-induced memory CD4 T cells with regard to proliferation rate and TCR repertoires. However, it is difficult to discriminate the first two nonconventional Th1 subsets, because there have been no specific markers or master regulators of their differentiation. Expression of PLZF, a transcription factor involved in NKT cells (31), was demonstrated in MP CD4 T cells in MHC class II transgenic mice, but they are not expressed in those in WT mice (32). Interestingly, it was recently reported that innate MP CD8 T cells and LIP-induced MP CD8 T cells showed a distinct pattern of gene expression (33). A similar approach would be applied for CD4 T cells in the future experiments.

Bystander activation of MP T cells is well recognized for CD8 T cells. We have also reported that naturally occurring MP CD8 T cells produce IFN-γ in response to IL-12 without antigenic stimulation (34). It was also shown that OVA-specific Tc1 cells were activated by IL-12 in the absence of the Ag (5). In contrast, there have been a few studies showing bystander activation of CD4 T cells, but one study showed IFN-γ production of naturally occurring MP CD4 T cells by stimulation with IL-12 in vitro or during *L. monocytogenes* infection in vivo (15). In this study, we extend these findings by demonstrating IL-12–induced IFN-γ

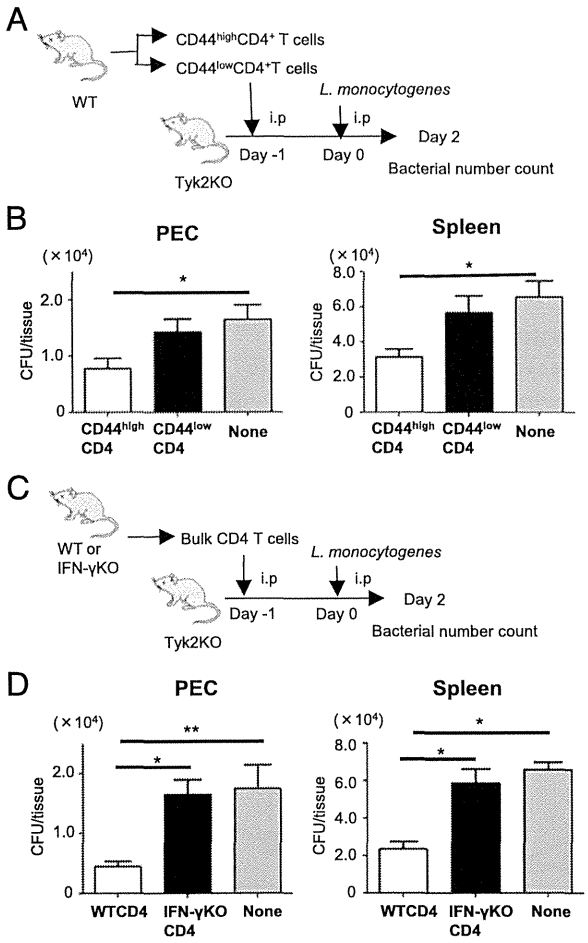

FIGURE 5. WT MP CD4 T cells confer protection against LM infection in Tyk2-deficient mice. (**A**) $CD44^{high}$ or $CD44^{low}$ $CD4^+$ T cells from WT mice were injected i.p. into Tyk2 KO (n = 5, in each group) mice 1 d before *L. monocytogenes* infection. Bacterial number in the peritoneal cavity (peritoneal exudate cells) and the spleen was measured 2 d after *L. monocytogenes* infection (**B**). (**C**) WT or IFN-γ KO CD4 T cells were injected i.p. into Tyk2 KO mice (n = 5, in each group) 1 d before *L. monocytogenes* infection. Bacterial number in the peritoneal cavity and the spleen was measured 2 d after *L. monocytogenes* infection (**D**). Data are mean ± SEM. $*p < 0.05$, $**p < 0.01$. Data are representative of three independent experiments.

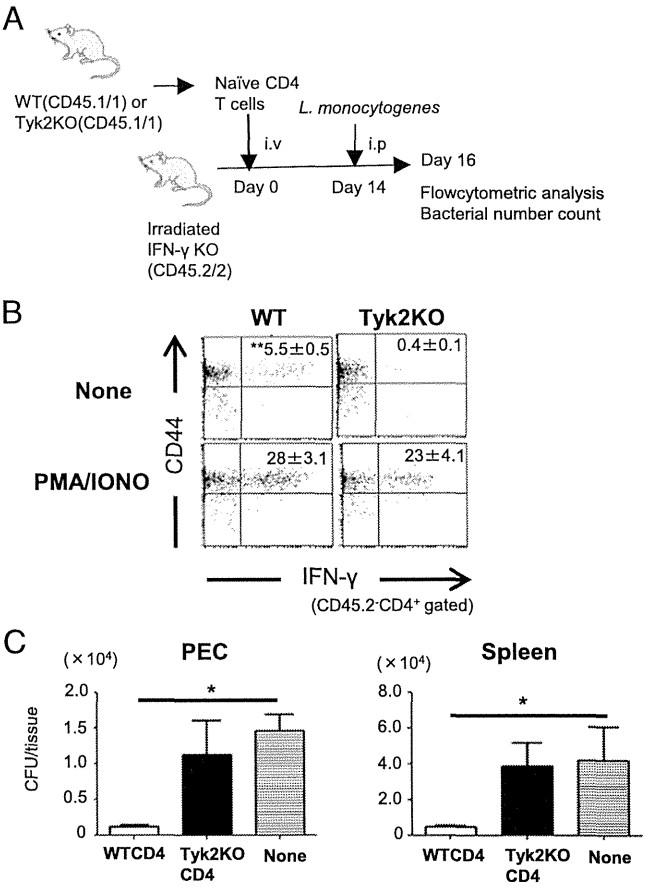

FIGURE 6. Tyk2-dependent innate host defense by LIP-induced Th1 cells. (**A**) Naive CD4 T cells from WT (CD45.1/1) or Tyk2 KO (CD45.1/1) mice were transferred i.v. into sublethally irradiated IFN-γ KO (Ly5.2/5.2) mice (n = 4 in each group). Two weeks after the transfer, the recipients were infected with *L. monocytogenes*, and the spleen and peritoneal exudate cells (PECs) were harvested from the recipient mice 2 d postinfection. (**B**) The PECs were cultured for 18 h without stimulation (*upper panels*) or stimulated with PMA and ionomycin for 5 h (*lower panels*) in the presence of brefeldin A; then the cells were tested for intracellular staining of IFN-γ. Representative dot plots are shown after gating on the donor $CD4^+$ cells. The numbers in the panels are the mean ± SEM percentages of IFN-γ^+ cells in $CD4^+$ cells. (**C**) Bacterial counts in the peritoneal cavity and the spleen of the recipient IFN-γ KO mice are shown. Data are mean ± SEM. $*p < 0.05$. Data are representative of two separate experiments.

production of Th1 cells generated by LIP and that of conventional Ag-induced Th1 cells. Thus, bystander activation is not a unique function of naturally occurring MP T cells, which might be called "innate-like" T cells, but rather a general feature of T cells expressing memory/activation markers.

It has been assumed that CD4 T cells participate in host defense against *L. monocytogenes* infection as a part of adaptive immune system specific for listerial Ags. However, it has also been known that listerial Ag-specific CD4 T cell responses become detectable when bacteria are almost eradicated (35). In addition, depleting CD4 T cells significantly increased bacterial burden from early stages after listerial infection (36, 37). Although an involvement of a small number of listerial Ag-specific CD4 T cells cannot be excluded, our data suggest an importance of IL-12–induced bystander IFN-γ production in CD4 T cell–mediated early host defense against *L. monocytogenes*. The degree of protection conferred by innate CD4 T cell activation was modest in the cell transfer experiments. This would have been improved by increasing the number of transferred CD4 T cells. However, it might overestimate their role, because CD4 T cells were not the main source of early IFN-γ production as shown in Fig. 4C. Nevertheless, it would be of interest to examine the relative importance of listerial Ag-specific CD4 T cells and bystander MP CD4 T cells during primary *L. monocytogenes* infection. The adaptive CD4 T cell responses might play a role only in secondary infection as memory CD4 T cells.

Berg et al. (5) demonstrated that OVA-specific CD8 T cells conferred protection against *L. monocytogenes* infection. In this study, we demonstrated in a similar system that OVA-specific CD4 T cells can confer protection against listerial infection through bystander IFN-γ production. This not only formally demonstrates that the CD4 T cell can be activated in an Ag-independent manner, but also indicates that cells in adaptive immune system can be involved in innate host defense. Thus, irrespective of whether CD4 or CD8 T cells, there is no difference in the innate functions not only in vitro but also in vivo between conventional Ag-induced effector/memory T cells and nonconventional T cells.

Our results indicate that Tyk2-mediated signaling in CD4 T cells is involved in both adaptive and innate host defense against intracellular pathogens. This is noteworthy because Tyk2 deficiency causes severe immune deficiency in humans (38). Although we examined only an acute infection model in this study, it is also

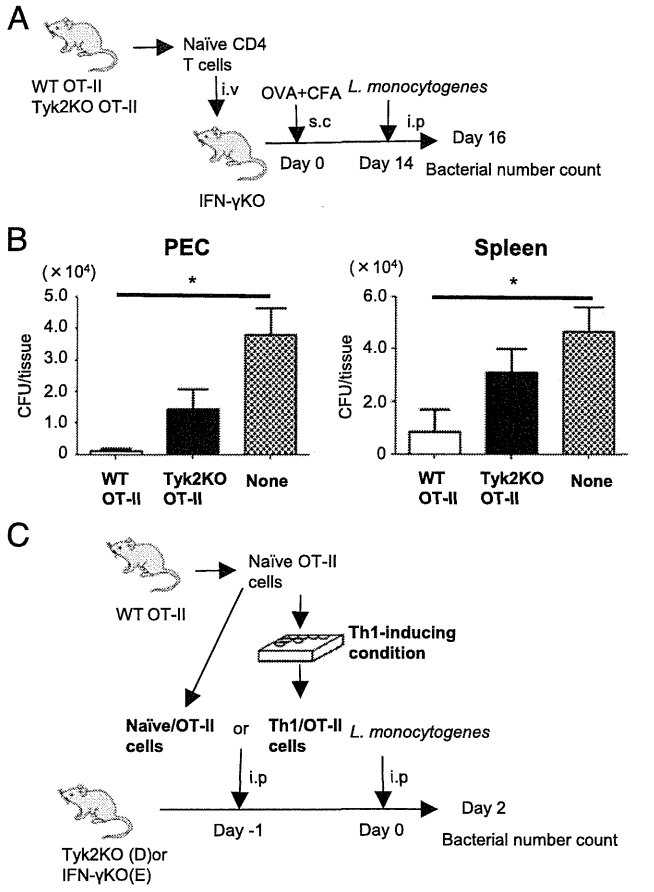

FIGURE 7. Bystander IFN-γ production of conventional Ag-induced Th1 cells can also confer protection against bacterial infection. (**A**) Naive CD4 T cells purified from WT or Tyk2 KO OT-II mice were transferred i.v. into IFN-γ KO mice ($n = 3$ in each group), which were immunized with OVA on the next day. Two weeks after immunization, the recipient mice were infected i.p. with *L. monocytogenes*, and the spleen and peritoneal exudate cells (PECs) were harvested on day 2 postinfection. (**B**) Bacterial number in the peritoneal cavity and the spleen are shown. Data are mean ± SEM. $^*p < 0.05$. (**C**) LNs cells from WT OT-II mice were stimulated with OVA peptide under a Th1-inducing condition for 4 d. Cells were collected and injected i.p. into Tyk2 KO or IFN-γ KO mice 1 d before *L. monocytogenes* infection. Control groups of mice were either transferred with the same number of naive OT-II cells or not receiving cell transfer. Bacterial number in the peritoneal cavity and the spleen of Tyk2 KO (**D**) or IFN-γ KO mice (**E**) was measured on day 2 postinfection. Data are mean ± SEM ($n = 3$ in each group). $^*p < 0.05$. Data are representative of three independent experiments.

possible that Tyk2-mediated bystander Th1 cell activation takes place during chronic infection and also in chronic inflammatory conditions such as autoimmunity. Thus, our data also provide important information for analyzing the Ag specificity of Th1 cells in the pathogenesis of these inflammatory diseases.

Disclosures

The authors have no financial conflicts of interest.

References

1. Pamer, E. G. 2004. Immune responses to *Listeria monocytogenes*. *Nat. Rev. Immunol.* 4: 812–823.
2. Dunn, P. L., and R. J. North. 1991. Early gamma interferon production by natural killer cells is important in defense against murine listeriosis. *Infect. Immun.* 59: 2892–2900.
3. Ranson, T., S. Bregenholt, A. Lehuen, O. Gaillot, M. C. Leite-de-Moraes, A. Herbelin, P. Berche, and J. P. Di Santo. 2005. Invariant V alpha 14+ NKT cells participate in the early response to enteric *Listeria monocytogenes* infection. *J. Immunol.* 175: 1137–1144.
4. Hiromatsu, K., Y. Yoshikai, G. Matsuzaki, S. Ohga, K. Muramori, K. Matsumoto, J. A. Bluestone, and K. Nomoto. 1992. A protective role of gamma/delta T cells in primary infection with *Listeria monocytogenes* in mice. *J. Exp. Med.* 175: 49–56.
5. Berg, R. E., E. Crossley, S. Murray, and J. Forman. 2003. Memory CD8+ T cells provide innate immune protection against *Listeria monocytogenes* in the absence of cognate antigen. *J. Exp. Med.* 198: 1583–1593.
6. Atherly, L. O., J. A. Lucas, M. Felices, C. C. Yin, S. L. Reiner, and L. J. Berg. 2006. The Tec family tyrosine kinases Itk and Rlk regulate the development of conventional CD8+ T cells. *Immunity* 25: 79–91.
7. Broussard, C., C. Fleischacker, R. Horai, M. Chetana, A. M. Venegas, L. L. Sharp, S. M. Hedrick, B. J. Fowlkes, and P. L. Schwartzberg. 2006. Altered development of CD8+ T cell lineages in mice deficient for the Tec kinases Itk and Rlk. [Published erratum appears in 2006 *Immunity* 25: 849.] *Immunity* 25: 93–104.
8. Hu, J., N. Sahu, E. Walsh, and A. August. 2007. Memory phenotype CD8+ T cells with innate function selectively develop in the absence of active Itk. *Eur. J. Immunol.* 37: 2892–2899.
9. Berg, L. J. 2007. Signalling through TEC kinases regulates conventional versus innate CD8(+) T-cell development. *Nat. Rev. Immunol.* 7: 479–485.
10. Lertmemongkolchai, G., G. Cai, C. A. Hunter, and G. J. Bancroft. 2001. Bystander activation of CD8+ T cells contributes to the rapid production of IFN-gamma in response to bacterial pathogens. *J. Immunol.* 166: 1097–1105.
11. Berg, R. E., C. J. Cordes, and J. Forman. 2002. Contribution of CD8+ T cells to innate immunity: IFN-gamma secretion induced by IL-12 and IL-18. *Eur. J. Immunol.* 32: 2807–2816.
12. Kambayashi, T., E. Assarsson, A. E. Lukacher, H. G. Ljunggren, and P. E. Jensen. 2003. Memory CD8+ T cells provide an early source of IFN-gamma. *J. Immunol.* 170: 2399–2408.
13. Su, J., R. E. Berg, S. Murray, and J. Forman. 2005. Thymus-dependent memory phenotype CD8 T cells in naive B6.H-2Kb$^{-/-}$Db$^{-/-}$ animals mediate an antigen-specific response against *Listeria monocytogenes*. *J. Immunol.* 175: 6450–6457.
14. Cho, B. K., V. P. Rao, Q. Ge, H. N. Eisen, and J. Chen. 2000. Homeostasis-stimulated proliferation drives naive T cells to differentiate directly into memory T cells. *J. Exp. Med.* 192: 549–556.
15. Hu, J., and A. August. 2008. Naive and innate memory phenotype CD4+ T cells have different requirements for active Itk for their development. *J. Immunol.* 180: 6544–6552.
16. Boyman, O. 2010. Bystander activation of CD4+ T cells. *Eur. J. Immunol.* 40: 936–939.
17. Younes, S. A., G. Punkosdy, S. Caucheteux, T. Chen, Z. Grossman, and W. E. Paul. 2011. Memory phenotype CD4 T cells undergoing rapid, nonburst-like, cytokine-driven proliferation can be distinguished from antigen-experienced memory cells. *PLoS Biol.* 9: e1001171.
18. Voehringer, D., H. E. Liang, and R. M. Locksley. 2008. Homeostasis and effector function of lymphopenia-induced "memory-like" T cells in constitutively T cell-depleted mice. *J. Immunol.* 180: 4742–4753.
19. Ghoreschi, K., A. Laurence, and J. J. O'Shea. 2009. Janus kinases in immune cell signaling. *Immunol. Rev.* 228: 273–287.
20. Shimoda, K., H. Tsutsui, K. Aoki, K. Kato, T. Matsuda, A. Numata, K. Takase, T. Yamamoto, H. Nukina, T. Hoshino, et al. 2002. Partial impairment of interleukin-12 (IL-12) and IL-18 signaling in Tyk2-deficient mice. *Blood* 99: 2094–2099.

21. Shimoda, K., K. Kato, K. Aoki, T. Matsuda, A. Miyamoto, M. Shibamori, M. Yamashita, A. Numata, K. Takase, S. Kobayashi, et al. 2000. Tyk2 plays a restricted role in IFN alpha signaling, although it is required for IL-12-mediated T cell function. *Immunity* 13: 561–571.
22. Karaghiosoff, M., H. Neubauer, C. Lassnig, P. Kovarik, H. Schindler, H. Pircher, B. McCoy, C. Bogdan, T. Decker, G. Brem, et al. 2000. Partial impairment of cytokine responses in Tyk2-deficient mice. *Immunity* 13: 549–560.
23. Li, W., H. Yamada, T. Yajima, R. Nakagawa, K. Shimoda, K. Nakayama, and Y. Yoshikai. 2007. Tyk2 signaling in host environment plays an important role in contraction of antigen-specific CD8+ T cells following a microbial infection. *J. Immunol.* 178: 4482–4488.
24. Pearce, E. L., and H. Shen. 2007. Generation of CD8 T cell memory is regulated by IL-12. *J. Immunol.* 179: 2074–2081.
25. Orgun, N. N., M. A. Mathis, C. B. Wilson, and S. S. Way. 2008. Deviation from a strong Th1-dominated to a modest Th17-dominated CD4 T cell response in the absence of IL-12p40 and type I IFNs sustains protective CD8 T cells. *J. Immunol.* 180: 4109–4115.
26. Oyamada, A., H. Ikebe, M. Itsumi, H. Saiwai, S. Okada, K. Shimoda, Y. Iwakura, K. I. Nakayama, Y. Iwamoto, Y. Yoshikai, and H. Yamada. 2009. Tyrosine kinase 2 plays critical roles in the pathogenic CD4 T cell responses for the development of experimental autoimmune encephalomyelitis. *J. Immunol.* 183: 7539–7546.
27. Aizu, K., W. Li, T. Yajima, T. Arai, K. Shimoda, Y. Nimura, and Y. Yoshikai. 2006. An important role of Tyk2 in APC function of dendritic cells for priming CD8+ T cells producing IFN-gamma. *Eur. J. Immunol.* 36: 3060–3070.
28. Itsumi, M., Y. Yoshikai, and H. Yamada. 2009. IL-15 is critical for the maintenance and innate functions of self-specific CD8(+) T cells. *Eur. J. Immunol.* 39: 1784–1793.
29. Trinchieri, G. 2003. Interleukin-12 and the regulation of innate resistance and adaptive immunity. *Nat. Rev. Immunol.* 3: 133–146.
30. Shibata, K., H. Yamada, T. Sato, T. Dejima, M. Nakamura, T. Ikawa, H. Hara, S. Yamasaki, R. Kageyama, Y. Iwakura, et al. 2011. Notch-Hes1 pathway is required for the development of IL-17-producing γδ T cells. *Blood* 118: 586–593.
31. Savage, A. K., M. G. Constantinides, J. Han, D. Picard, E. Martin, B. Li, O. Lantz, and A. Bendelac. 2008. The transcription factor PLZF directs the effector program of the NKT cell lineage. *Immunity* 29: 391–403.
32. Lee, Y. J., Y. K. Jeon, B. H. Kang, D. H. Chung, C. G. Park, H. Y. Shin, K. C. Jung, and S. H. Park. 2010. Generation of PLZF+ CD4+ T cells via MHC class II-dependent thymocyte-thymocyte interaction is a physiological process in humans. *J. Exp. Med.* 207: 237–246.
33. Huang, W., J. Hu, and A. August. 2013. Cutting edge: innate memory CD8+ T cells are distinct from homeostatic expanded CD8+ T cells and rapidly respond to primary antigenic stimuli. *J. Immunol.* 190: 2490–2494.
34. Yajima, T., H. Nishimura, R. Ishimitsu, K. Yamamura, T. Watase, D. H. Busch, E. G. Pamer, H. Kuwano, and Y. Yoshikai. 2001. Memory phenotype CD8(+) T cells in IL-15 transgenic mice are involved in early protection against a primary infection with *Listeria monocytogenes*. *Eur. J. Immunol.* 31: 757–766.
35. Zenewicz, L. A., and H. Shen. 2007. Innate and adaptive immune responses to *Listeria monocytogenes*: a short overview. *Microbes Infect.* 9: 1208–1215.
36. Umeda, K., X. Sun, Y. Guo, H. Yamada, K. Shibata, and Y. Yoshikai. 2011. Innate memory phenotype CD4+ T cells play a role in early protection against infection by *Listeria monocytogenes* in a CD30L-dependent manner. *Microbiol. Immunol.* 55: 645–656.
37. Czuprynski, C. J., J. F. Brown, K. M. Young, and A. J. Cooley. 1989. Administration of purified anti-L3T4 monoclonal antibody impairs the resistance of mice to *Listeria monocytogenes* infection. *Infect. Immun.* 57: 100–109.
38. Minegishi, Y., M. Saito, T. Morio, K. Watanabe, K. Agematsu, S. Tsuchiya, H. Takada, T. Hara, N. Kawamura, T. Ariga, et al. 2006. Human tyrosine kinase 2 deficiency reveals its requisite roles in multiple cytokine signals involved in innate and acquired immunity. *Immunity* 25: 745–755.

THE JOURNAL OF BIOLOGICAL CHEMISTRY VOL. 289, NO. 19, pp. 12946–12961, May 9, 2014

Protrudin Regulates Endoplasmic Reticulum Morphology and Function Associated with the Pathogenesis of Hereditary Spastic Paraplegia*

Received for publication, October 19, 2013, and in revised form, March 17, 2014 Published, JBC Papers in Press, March 25, 2014, DOI 10.1074/jbc.M113.528687

Yutaka Hashimoto[1], **Michiko Shirane**[1,2], **Fumiko Matsuzaki, Shotaro Saita, Takafumi Ohnishi, and Keiichi I. Nakayama**

From the Department of Molecular and Cellular Biology, Medical Institute of Bioregulation, Kyushu University, 3-1-1 Maidashi, Higashi-ku, Fukuoka, Fukuoka 812-8582, Japan

Background: Certain hereditary spastic paraplegia (HSP)-related proteins possess hairpin domains and regulate the morphology of the endoplasmic reticulum (ER) network.
Results: Protrudin possesses a hairpin domain and interacts with HSP-related proteins.
Conclusion: Protrudin regulates ER morphology and function.
Significance: Mutant protrudin produced in certain individuals with HSP is prone to form microaggregates that induce ER stress.

Protrudin is a membrane protein that regulates polarized vesicular trafficking in neurons. The protrudin gene (*ZFYVE27*) is mutated in a subset of individuals with hereditary spastic paraplegia (HSP), and protrudin is therefore also referred to as spastic paraplegia (SPG) 33. We have now generated mice that express a transgene for dual epitope-tagged protrudin under control of a neuron-specific promoter, and we have subjected highly purified protrudin-containing complexes isolated from the brain of these mice to proteomics analysis to identify proteins that associate with protrudin. Protrudin was found to interact with other HSP-related proteins including myelin proteolipid protein 1 (SPG2), atlastin-1 (SPG3A), REEP1 (SPG31), REEP5 (similar to REEP1), Kif5A (SPG10), Kif5B, Kif5C, and reticulon 1, 3, and 4 (similar to reticulon 2, SPG12). Membrane topology analysis indicated that one of three hydrophobic segments of protrudin forms a hydrophobic hairpin domain similar to those of other SPG proteins. Protrudin was found to localize predominantly to the tubular endoplasmic reticulum (ER), and forced expression of protrudin promoted the formation and stabilization of the tubular ER network. The protrudin(G191V) mutant, which has been identified in a subset of HSP patients, manifested an increased intracellular stability, and cells expressing this mutant showed an increased susceptibility to ER stress. Our results thus suggest that protrudin contributes to the regulation of ER morphology and function, and that its deregulation by mutation is a causative defect in HSP.

The endoplasmic reticulum (ER)[3] is a continuous membrane system that comprises the nuclear envelope, ribosome-studded peripheral sheets, and an interconnected network of smooth tubules that extend throughout the cell. The ER is a multifunctional organelle that plays a key role in the synthesis, modification, quality control, and trafficking of integral membrane and secreted proteins (1, 2). It also contributes to Ca^{2+} sequestration and release, cellular signaling, sterol synthesis, as well as lipid synthesis and distribution. In neurons, the ER participates in the massive polarized membrane expansion that occurs during axon and dendrite formation as well as serves as an intracellular Ca^{2+} store that is integrated into pre- and postsynaptic signaling pathways (3).

Hereditary spastic paraplegia (HSP) is an inherited neurological disorder characterized by spastic weakness of the lower extremities (4–6). More than half of HSP cases result from autosomal dominant mutations in the genes for atlastin-1 (also known as spastic paraplegia 3A, or SPG3A), receptor expression enhancing protein (REEP) 1 (SPG31), and spastin (SPG4). Atlastin-1, spastin, and REEP1 interact with each other in the tubular ER membrane of neurons to coordinate ER morphogenesis and microtubule dynamics (7). These three proteins as well as reticulon 2 (SPG12) possess hydrophobic hairpin domains that shape high-curvature ER tubules and mediate intramembrane protein interactions (8). Members of the atlastin/RHD3/Sey1 family of dynamin-related GTPases mediate the formation of three-way junctions that characterize the tubular ER network (9–11), and additional classes of hydrophobic hairpin-containing ER proteins interact with and remodel the microtubule cytoskeleton. Indeed, overexpression or depletion of these various proteins affects ER morphology (10, 12, 13), and abnormal ER morphology is thought to be a major causative defect in HSP pathogenesis.

Protrudin (*ZFYVE27* or *SPG33*) was also identified as a protein whose gene is mutated in a subset of HSP patients (14).

* This work was supported in part by a Japan Society for the Promotion of Science KAKENHI Grant-in-Aid for Young Scientists (S) (to M. S.).
[1] Both authors contributed equally to this work.
[2] To whom correspondence should be addressed. Tel.: 81-92-642-6816; Fax: 81-92-642-6819; E-mail: smichi@bioreg.kyushu-u.ac.jp.
[3] The abbreviations used are: ER, endoplasmic reticulum; HSP, hereditary spastic paraplegia; SPG, spastic paraplegia; REEP, receptor expression enhancing protein; VAP, vesicle-associated membrane protein-associated protein; PLP1, myelin proteolipid protein 1; UPR, unfolded protein response; Ni-NTA, nickel-nitrilotriacetic acid; OMIM, Online Mendelian Inheritance in Man; mPEG, methoxypolyethylene glycol maleimide; XBP1, X-box binding protein 1; ALS, amyotrophic lateral sclerosis; EGFP, enhanced green fluorescent protein; ERAD, ER-associated degradation.

Protrudin contains a Rab11 binding domain and a FYVE domain, and promotes neurite formation through activation of polarized vesicular trafficking (15). Protrudin also contains a short sequence motif designated FFAT (two phenylalanines in an acidic tract) between the Rab11 binding domain and the FYVE domain, and this motif mediates the interaction of protrudin with vesicle-associated membrane protein-associated protein (VAP) (16) as well as with Kif5A (SPG10), a motor protein that mediates anterograde vesicular transport in neurons. VAP is an important determinant of the subcellular localization of protrudin at the ER. Protrudin facilitates the interaction of Kif5 with Rab11, VAP family proteins, Surf4, and reticulon proteins, suggesting that it serves as an adaptor protein and that the protrudin-Kif5 complex contributes to the transport of these proteins in neurons (17). Given that mutations in the genes for protrudin, Kif5A, and reticulons give rise to HSP, protrudin-containing complexes appear to be fundamental to neuronal function associated with HSP pathogenesis.

To identify proteins that engage in physiologically relevant interactions with protrudin in the central nervous system, we generated mice that express a protrudin transgene under control of a neuron-specific prion promoter. We isolated protrudin complexes from the brain of these animals and identified component proteins by proteomics analysis. We now show that protrudin is associated with major HSP-related proteins including myelin proteolipid protein 1 (PLP1, SPG2); reticulon 1, 3, and 4; atlastin-1; REEP1 and REEP5; and Kif5A, -B, and -C. Protrudin was found to colocalize with atlastin-1, REEP1, and REEP5 at the tubular ER network, and overexpression of protrudin promoted the formation and stabilization of this network. Topological analysis revealed that protrudin possesses a hydrophobic hairpin domain similar to those of other HSP-related ER-shaping proteins. A mutant (G191V) of protrudin that is associated with HSP in a subset of patients was found to have an increased intracellular stability and to increase the sensitivity of cells to ER stress. Our results thus suggest that protrudin contributes to formation of the ER network and that altered protrudin function contributes to the pathology of HSP.

EXPERIMENTAL PROCEDURES

Generation of Protrudin Transgenic Mice—Animals were handled in accordance with the guidelines of Kyushu University. A cDNA for mouse protrudin with the His_6 and FLAG epitopes at its NH_2 terminus was subcloned into the pPrPpE1/E2,3sal plasmid, which contains a prion promoter. The resulting vector was linearized and injected into fertilized mouse eggs of the (C57BL/6NCrSlc × DBA/2CrSlc)F1 (BDF1) background. Primary genotyping was performed by PCR and Southern blot analysis and was followed by immunoblot analysis with antibodies to (anti-) FLAG. WT littermates of the transgenic mice were studied as controls.

Construction of Expression Plasmids—Construction of vectors encoding human protrudin (15) and VAP-A(ΔTM) (16), as well as mouse protrudin (17), was described previously. Mouse cDNAs encoding atlastin-1, REEP5, REEP1, and VAP-A were generated by PCR with PrimeSTAR HS DNA polymerase (Takara, Shiga, Japan) from cDNA prepared from Neuro2A cells. Human cDNAs encoding Sec61β and Climp63 were generated by PCR from cDNA prepared from HeLa cells. The cDNAs encoding mouse atlastin-1, REEP5, REEP1, and VAP-A were subcloned into pEFBOS-HHg (kindly provided by S. Nagata, Kyoto University, Japan, and H. Sumimoto, Kyushu University, Japan). Complementary DNAs encoding deletion mutants of human protrudin were generated by PCR and subcloned into p3xFLAG-CMV-7.1 (Sigma), and those encoding deletion mutants of mouse protrudin tagged with the HA and Myc epitopes at their NH_2 and COOH termini, respectively, were generated by PCR and subcloned into the pEFBOS vector. The cDNA encoding human Sec61β was subcloned into pEFBOS-HHg or ptdTomato (Clontech, Palo Alto, CA), and that encoding human Climp63 was subcloned into pEGFP (Clontech). The cDNAs encoding WT or G191V mutant forms of human protrudin tagged with the HA epitope were subcloned into pMX-puro (kindly provided by T. Kitamura, Tokyo University, Japan). The pcDNA3-NHK-FLAG vector was kindly provided by H. Ichijo, Tokyo University, Japan.

Antibodies—Antibodies to protrudin and FKBP38 were generated as described previously (15, 18). Antibodies to GM130 and heat shock protein 90 (HSP90) were from BD Biosciences; FLAG (mouse monoclonal M2 and rabbit polyclonal) and the Myc epitope (9E10) were from Sigma; HA epitope (HA.11) were from Covance (Princeton, NJ); α-tubulin (TU-01) from Zymed Laboratories Inc. (South San Francisco, CA); calreticulin from Thermo Scientific (Rockford, IL); Climp63 (clone G1/296) from Enzo Life Science (Farmingdale, NY); calnexin (N and C epitopes) from Stressgen (Victoria, British Columbia, Canada); protrudin from Proteintech (Chicago, IL); and HA epitope (Y-11) and cyclin D1-(72–13G) as well as normal mouse IgG (sc-2025) from Santa Cruz Biotechnology (Santa Cruz, CA). Alexa Fluor 488- or Alexa Fluor 546-conjugated goat antibodies to mouse or rabbit IgG were obtained from Molecular Probes (Eugene, OR).

Cell Culture, Transfection, and Retroviral Infection—Neuro2A, HEK293T, HeLa, COS-7, and Plat-E cells were cultured under a humidified atmosphere of 5% CO_2 at 37 °C in DMEM (Invitrogen) supplemented with 10% FBS (Invitrogen). The culture medium for Plat-E cells was also supplemented with blasticidin (10 μg/ml). Cells were transfected with the use of the FuGENE HD (Roche Applied Science) or Lipofectamine 2000 (Invitrogen) reagents. For retroviral infection, Plat-E cells were transiently transfected with pMX-puro-based vectors and then cultured for 48 h. The retroviruses in the resulting culture supernatants were used to infect Neuro2A cells, and the cells were then subjected to selection with puromycin (1 μg/ml). The infected cells were incubated with tunicamycin (Sigma), thapsigargin (Sigma), or DTT (Sigma) to induce the unfolded protein response (UPR), and exposed to cycloheximide (Sigma) to inhibit protein synthesis or MG132 (Sigma) to inhibit proteasome activity. Nocodazole was obtained from Sigma.

Isolation of Protrudin Complexes by Dual Affinity Purification—The brains of protrudin transgenic mice were disrupted with a Potter homogenizer, the homogenate was centrifuged at 1000 × *g* for 5 min at 4 °C to remove nuclei and nondisrupted cells, and the resulting supernatant was centrifuged at 100,000 × *g* for 30 min at 4 °C to isolate a membrane pellet. The pellet was solubilized with lysis buffer (40 mM HEPES-NaOH

(pH 7.5), 150 mM NaCl, 10% glycerol, 0.5% Triton X-100, 1 mM Na_3VO_4, 25 mM NaF, aprotinin (10 μg/ml), leupeptin (10 μg/ml), 1 mM PMSF). The protein concentration of the resulting supernatant was determined with the Bradford assay (Bio-Rad), and this soluble membrane fraction was then incubated with rotation for 60 min at 4 °C with anti-FLAG (M2)-agarose affinity gel (Sigma). The beads were washed three times with lysis buffer, after which protein complexes were eluted by incubation for several minutes at 4 °C with lysis buffer containing the FLAG peptide (Sigma). For the second affinity purification step, nickel-nitrilotriacetic acid (Ni-NTA)-agarose (ProBond resin, Invitrogen) was added to the eluate, and the mixture was incubated with rotation for 90 min at 4 °C. The beads were washed three times with lysis buffer, and protein complexes were eluted by incubation for several minutes at 4 °C with lysis buffer containing 300 mM imidazole.

Identification of Protrudin-associated Proteins by LC-MS/MS Analysis—LC-MS/MS analysis was performed as described previously (17). Proteins reproducibly detected in both of two independent experiments with brain extract from protrudin transgenic mice, but not with that from nontransgenic mice, were considered protrudin-associated proteins (17). Subcellular categorization was based on gene ontology annotation with the Mouse Genome Informatics (MGI) GO Term Finder. Genes responsible for HSP or other neurodegenerative diseases were based on Online Mendelian Inheritance in Man (OMIM) data. Semiquantitative estimation of protein abundance was based on identification frequency (19), which was normalized by the sum of the identification frequencies for all identified proteins in each experiment and then multiplied by 100 (17).

Immunoprecipitation and Immunoblot Analysis—HEK293T cells cultured for 1 day after transfection were lysed by incubation for 10 min at 4 °C with a lysis buffer (40 mM HEPES-NaOH (pH 7.5), 150 mM NaCl, 10% glycerol, 0.5% CHAPS, 1 mM Na_3VO_4, 25 mM NaF, aprotinin (10 μg/ml), leupeptin (10 μg/ml), 1 mM PMSF). The lysates were centrifuged at 20,400 × *g* for 10 min at 4 °C, and equal amounts of protein from the resulting supernatants were subjected to immunoblot analysis directly or to immunoprecipitation for 30 min at 4 °C with anti-FLAG and protein G-Sepharose 4 Fast Flow (Amersham Biosciences). The immunoprecipitates were washed three times with lysis buffer and then subjected to immunoblot analysis as described previously (15). The blot images were scanned with a LAS-4000 instrument (GE Healthcare), and the intensity of immunoblot bands was quantified with the use of ImageJ software.

Immunostaining and Image Analysis—HeLa or COS-7 cells were fixed for 10 min at room temperature with 4% paraformaldehyde in PBS before consecutive incubation with primary antibodies and Alexa Fluor 488- or Alexa Fluor 546-labeled goat secondary antibodies in PBS containing 1% Triton X-100. They were also stained with Hoechst 33258 (Wako, Tokyo, Japan) in some experiments. Cells were covered with a drop of GEL/MOUNT (Biomeda, Hayward, CA) and examined with a fluorescence microscope (Olympus BX51) or a laser-scanning confocal microscope (LSM510; Carl Zeiss, Oberkochen, Germany). The PSC colocalization plug-in for ImageJ was used to quantify Pearson's correlation coefficient for signals in two channels in the selected region. The default threshold value of 40 for 8-bit images, which was above the background fluorescence, was used for quantification in both channels. The density of three-way junctions of ER was quantified on the basis of the number of empty spaces surrounded by ER in a selected square area of 200 μm^2. The empty spaces were counted manually.

Subcellular Fractionation—The brains of WT or protrudin-deficient mice were homogenized in a solution containing 20 mM HEPES-NaOH (pH 7.4), 0.32 M sucrose, 1 mM Na_3VO_4, 25 mM NaF, aprotinin (10 μg/ml), leupeptin (10 μg/ml), 10 μM MG132, 1 mM PMSF, and 1 mM EDTA. The homogenate was centrifuged at 500 × *g* for 5 min at 4 °C to remove debris, and the resulting supernatant was then centrifuged at 100,000 × *g* for 1 h at 4 °C to obtain cytosolic and membrane fractions.

Sodium Carbonate Extraction—HEK293T cells transfected with a vector for HA-protrudin-Myc were cultured for 1 day, washed with PBS, and homogenized in an alkaline solution (0.25 M sucrose, 0.1 M sodium carbonate (pH 11.4), 1 mM Na_3VO_4, 25 mM NaF, aprotinin (10 μg/ml), leupeptin (10 μg/ml), 10 μM MG132, 1 mM PMSF). The homogenate was centrifuged at 100,000 × *g* for 1 h at 4 °C, and the resulting pellet was resuspended in a lysis buffer (40 mM HEPES-NaOH (pH 7.5), 150 mM NaCl, 10% glycerol, 0.5% Triton X-100, 1 mM Na_3VO_4, 25 mM NaF, aprotinin (10 μg/ml), leupeptin (10 μg/ml), 1 mM PMSF).

Protease Protection Assay—HEK293T cells transfected with WT or mutant forms of HA-protrudin-Myc were cultured for 1 day, washed with PBS, and homogenized in a solution identical to that used for subcellular fractionation with the exception that the sucrose concentration was 0.25 M. The homogenate was centrifuged at 500 × *g* for 5 min at 4 °C to remove debris, and the resulting supernatant was centrifuged at 100,000 × *g* for 1 h at 4 °C. The new pellet was suspended in 0.25 M sucrose buffer and incubated for 20 min on ice with proteinase K (40 μg/ml, Roche Applied Science) in the absence or presence of 1% Triton X-100. Proteolysis was terminated by the addition of PMSF to a final concentration of 1 mM.

Chemical Modification with mPEG—HeLa cells expressing mutant forms of protrudin tagged at the NH_2 terminus with the HA epitope were harvested by exposure to trypsin and then washed twice with DMEM and once with ice-cold HCN buffer (50 mM HEPES-NaOH (pH 7.5), 2 mM $CaCl_2$, 150 mM NaCl). They were then incubated for 20 min at 4 °C in HCN buffer containing 0.04% digitonin (to permeabilize the plasma membrane) or 0.1% Triton X-100 (to permeabilize all cell membranes), washed twice with ice-cold HNE buffer (50 mM HEPES-NaOH (pH 7.5), 150 mM NaCl, 1 mM EGTA), and transferred to a new tube. They were then incubated first for 10 min at 37 °C in HNE buffer and then for 30 min at 30 °C with 1.5 mM methoxypolyethylene glycol maleimide (mPEG, Sigma) in 20 mM Tris-HCl (pH 7.5). The reaction was terminated by the addition of DTT to a final concentration of 10 mM and incubation for 10 min at 4 °C. The cells were lysed by incubation for 20 min at 4 °C with lysis buffer (50 mM HEPES-NaOH (pH 7.5), 150 mM NaCl, 2 mM $CaCl_2$, 1% Triton X-100, aprotinin (10 μg/ml), leupeptin (10 μg/ml), 1 mM PMSF), after which the

lysates were centrifuged at 20,400 × *g* for 10 min at 4 °C and the resulting supernatant was subjected to immunoblot analysis.

RNAi—Stealth siRNAs designed for human protrudin (*ZFYVE27*, 5′-AGGAUGCAGGUGAUGGUGUUCGAUA-3′ and 5′-AAGAAGAGGCGGAGCUGCAGUAAUU-3′; numbers 1 and 2, respectively) or negative control duplexes (Invitrogen) were introduced into HeLa cells by transfection with Lipofectamine RNAiMax (Invitrogen). For rescue experiments, plasmids were introduced into the cells by transfection 2 days after the siRNAs.

RT and Real-time PCR Analysis—Total RNA was isolated from Neuro2A cells and purified with the use of an RNeasy Plus Mini Kit (Qiagen, Hilden, Germany). Portions of the RNA were subjected to RT with the use of a QuantiTect RT kit (Qiagen), and the resulting cDNA was subjected to real-time PCR analysis with a StepOne real-time PCR system (Applied Biosystems, Foster City, CA) and SYBR Premix Ex Taq (Takara). The amplification protocol comprised the initial incubation at 60 °C for 30 s and 95 °C for 3 s, followed by 40 cycles of denaturation, annealing, and extension. Data were analyzed according to the $2^{-\Delta\Delta CT}$ method and were normalized relative to the amount of GAPDH mRNA. PCR was performed with primers (forward and reverse, respectively) for mouse *Gapdh* (5′-CATGGCCTTCCGTGTTCCTA-3′ and 5′-GCGGCACGTCAGATCCA-3′) and mouse *Bip* (5′-TCTCACTAAAATGAAGGAGA-3′ and 5′-TTGTCGCTGGGCATCATTGA-3′).

Luciferase Assay—Neuro2A cells were transfected with pGL3-GRP78P(−132)-luc (kindly provided by K. Mori, Kyoto University) as an ER stress response element reporter together with pRL-TK (Promega, Madison, WI). The cells were collected 24 h after transfection, lysed, and assayed for luciferase activity with a dual-luciferase reporter assay system (Promega).

XBP1 mRNA Splicing Assay—Total RNA was isolated from Neuro2A cells and purified with the use of ISOGEN (Nippon Gene, Tokyo, Japan). Portions of the RNA were subjected to RT with the use of a QuantiTect RT kit (Qiagen), and the resulting cDNA was subjected to PCR with primers (forward and reverse, respectively) for mouse *Hprt* (hypoxanthine-guanine phosphoribosyltransferase) (*Hprt*, 5′-GCCTAAGATGAGCGCAAGTTG-3′ and 5′-TACTAGGCAGATGGCCACAGG-3′) and mouse X-box binding protein 1 (*Xbp1*, 5′-ACACGCTTGGGAATGGACAC-3′ and 5′-CCATGGGAAGATGTTCTGGG-3′) followed by agarose gel electrophoresis and staining with ethidium bromide. The gels were scanned with a LAS-4000 instrument, and band intensity was quantified with the use of ImageJ software.

Gel Filtration Chromatography—Gel filtration chromatography was performed with an ÄKTAexplorer 10S system (GE Healthcare) fitted with a Superose 6 10/300 GL column (GE Healthcare). Cells were lysed by incubation for 10 min at 4 °C with a lysis buffer (50 mM sodium phosphate (pH 7.5), 150 mM NaCl, 10% glycerol, 1% CHAPS, 1 mM Na_3VO_4, 25 mM NaF, aprotinin (10 μg/ml), leupeptin (10 μg/ml), 1 mM PMSF). The lysates were centrifuged at 20,400 × *g* for 10 min at 4 °C, and equal amounts of protein from the resulting supernatants were injected into the column equilibrated with running buffer (50 mM sodium phosphate (pH 7.5), 150 mM NaCl, 10% glycerol, 1% CHAPS). Elution was performed at a flow rate of 0.4 ml/min, and 0.48 ml fractions were collected.

Statistical Analysis—Where indicated, quantitative data are presented as mean ± S.D. and analyzed by Student's *t* test or by one-way analysis of variance followed by Tukey's test. A p value of <0.05 was considered statistically significant.

RESULTS

Identification of Protrudin-interacting Proteins in Mouse Brain—To provide further insight into the physiological role of protrudin, we generated transgenic mice that express a form of protrudin tagged with both His_6 and FLAG epitopes under control of a neuron-specific prion promoter (Fig. 1*A*). Protrudin-containing complexes were purified from the brain of these transgenic mice by tandem affinity chromatography with anti-FLAG and Ni-NTA resin (which binds to the His_6 epitope). Proteins in the final eluate were digested with trypsin, and the generated peptides were subjected to LC-MS/MS. We identified 141 proteins that were present in the complexes isolated from the transgenic mice but were not recovered from control mice (Fig. 1*A*). Assignment of the protrudin-associated proteins to subcellular compartments on the basis of gene ontology annotation with the use of the Mouse Genome Informatics (MGI) GO Term Finder revealed that more than half of these proteins were localized at the plasma membrane or ER (Fig. 1*B*, Table 1), consistent with the notion that protrudin plays an important role in the endomembrane system. Given that protrudin is implicated in the pathogenesis of HSP, protrudin-associated proteins were categorized on the basis of OMIM annotation. A substantial proportion (11.1%) of the proteins implicated in HSP pathology were found in protrudin complexes, whereas <5% of those related to other neurodegenerative diseases, such as amyotrophic lateral sclerosis (ALS), Charcot-Marie-Tooth disease, Parkinsons disease, and spinocerebellar ataxia, were detected in these complexes (Fig. 1*C*, Table 2). All protrudin-associated proteins directly implicated in or potentially related to HSP were subjected to semiquantitative analysis on the basis of the normalized identification frequency in each LC-MS/MS experiment (Fig. 1*D*). PLP1 and several reticulon family members ranked high in the list, and altastin-1, REEP5, and Kif5 isoforms were also identified. In addition, REEP1 was identified as a protein that interacts with protrudin by proteomics analysis of immunoprecipitates prepared from the brain of C57BL/6 mice with anti-protrudin (data not shown; see also Fig. 2, *C* and *F*). These results suggested that protrudin forms complexes with many HSP-related proteins.

Protrudin Associates with Atlastin-1, REEP5, and REEP1 at the ER Network—To confirm the interaction of protrudin with atlastin-1, REEP5, and REEP1, we performed co-immunoprecipitation analysis. Lysates of HEK293T cells transfected with expression vectors for both FLAG-tagged mouse protrudin and HA epitope-tagged forms of mouse atlastin-1, REEP5, REEP1, VAP-A (positive control), or a VAP-A mutant (ΔTM) lacking the transmembrane domain (negative control) were subjected to immunoprecipitation with anti-FLAG. The resulting precipitates were then subjected to immunoblot analysis with anti-HA and anti-FLAG. Atlastin-1 (Fig. 2*A*), REEP5 (Fig. 2*B*), and REEP1 (Fig. 2*C*) were detected in the FLAG-protrudin

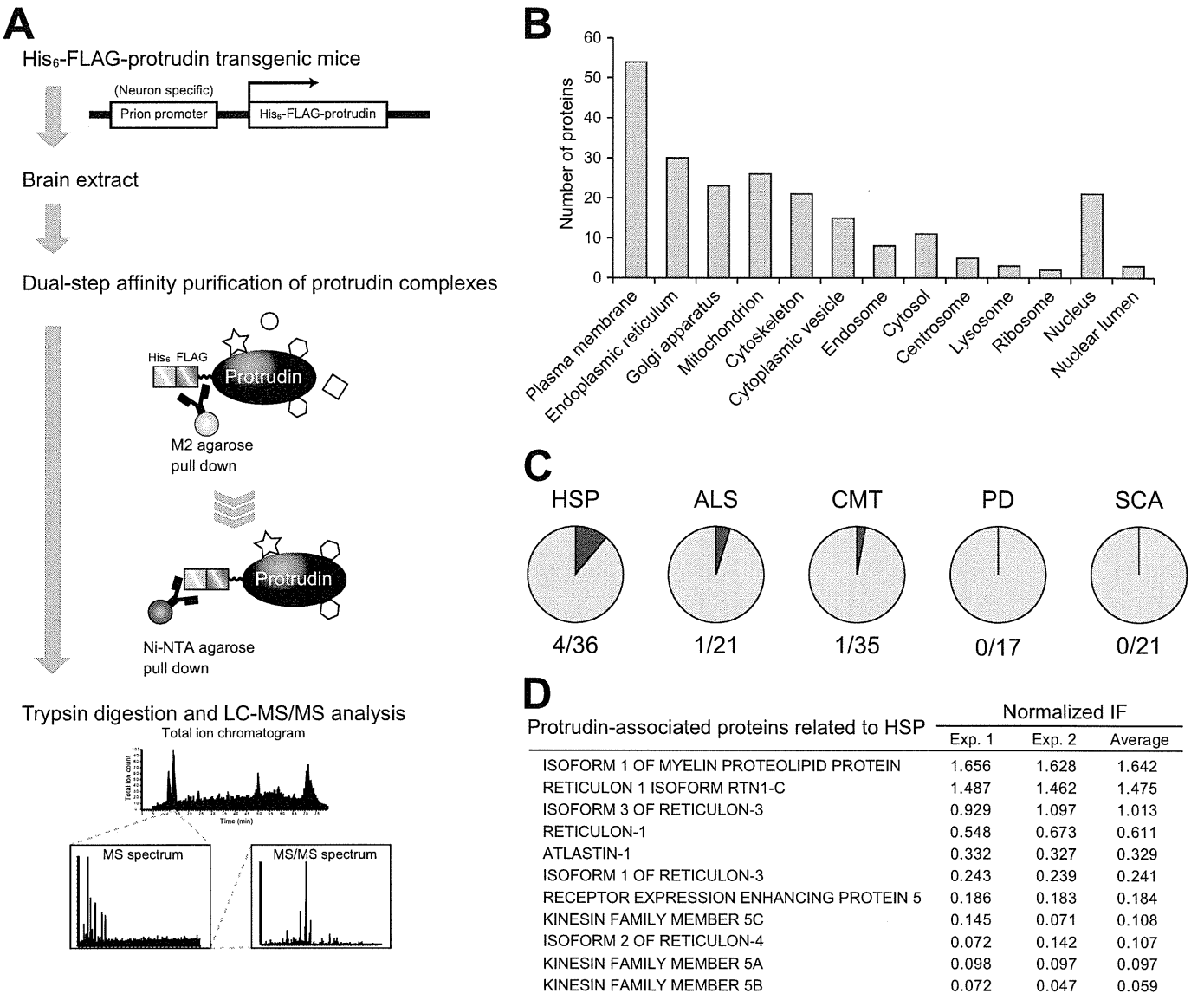

D

Protrudin-associated proteins related to HSP	Normalized IF		
	Exp. 1	Exp. 2	Average
ISOFORM 1 OF MYELIN PROTEOLIPID PROTEIN	1.656	1.628	1.642
RETICULON 1 ISOFORM RTN1-C	1.487	1.462	1.475
ISOFORM 3 OF RETICULON-3	0.929	1.097	1.013
RETICULON-1	0.548	0.673	0.611
ATLASTIN-1	0.332	0.327	0.329
ISOFORM 1 OF RETICULON-3	0.243	0.239	0.241
RECEPTOR EXPRESSION ENHANCING PROTEIN 5	0.186	0.183	0.184
KINESIN FAMILY MEMBER 5C	0.145	0.071	0.108
ISOFORM 2 OF RETICULON-4	0.072	0.142	0.107
KINESIN FAMILY MEMBER 5A	0.098	0.097	0.097
KINESIN FAMILY MEMBER 5B	0.072	0.047	0.059

FIGURE 1. **Identification of protrudin-associated proteins with a proteomics approach.** *A*, schematic workflow for identification of protrudin-associated proteins by proteomics analysis. An extract prepared from the brain of protrudin transgenic mice was subjected to dual affinity purification with anti-FLAG and Ni-NTA-agarose. The isolated protrudin complexes were subjected to SDS-PAGE, slices of the resulting gel were exposed to trypsin, and the generated peptides were analyzed by LC-MS/MS. The mass and partial amino acid sequence data were simultaneously compared with protein and nucleotide sequence databases for protein identification. *B*, subcellular localization of protrudin-associated proteins identified by LC-MS/MS analysis. *C*, proportion of proteins encoded by genes responsible for the indicated diseases in OMIM that were identified in protrudin complexes. *D*, proteins directly implicated in or potentially related to HSP identified in *A*. The amount of each protein was estimated semiquantitatively on the basis of the normalized identification frequency (*IF*). The proteins were ranked according to the average of the scores from two independent experiments (*Exp. 1* and *Exp. 2*).

immunoprecipitates. We next examined the subcellular localization of these proteins in HeLa cells. FLAG-tagged protrudin was colocalized with HA-tagged atlastin-1 (Fig. 2*D*), HA-REEP5 (Fig. 2*E*), and HA-REEP1 (Fig. 2*F*) at tubular and reticular structures, suggesting that protrudin forms complexes with atlastin-1, REEP5, and REEP1 in the tubular ER network.

We next investigated which region of protrudin is required for binding to atlastin-1 or REEP5 by generating FLAG-tagged deletion mutants of protrudin (Fig. 2*G*) and examining their ability to associate with HA-tagged atlastin-1 (Fig. 2*H*) or HA-REEP5 (Fig. 2*I*) in a co-immunoprecipitation assay with HEK293T cells. Whereas full-length protrudin and a mutant that included the NH_2-terminal region of protrudin (amino acids 1 to 206) interacted with atlastin-1 and REEP5, a mutant that lacked this region failed to do so, suggesting that the NH_2-terminal half of protrudin including three putative hydrophobic domains is necessary and sufficient for the interaction of protrudin with either atlastin-1 or REEP5.

Protrudin Is an Integral Membrane Protein—In silico analysis with SMART (Simple Modular Architecture Research Tool) suggested that protrudin contains three hydrophobic or transmembrane domains. Cytosolic and membrane fractions prepared from the brain of WT or protrudin knock-out mice were subjected to immunoblot analysis with anti-protrudin. Protrudin was detected in the membrane fraction but not in the cytosolic fraction of WT mice (Fig. 3*A*). We next investigated whether protrudin is substantially integrated in or simply attached to cellular membranes. HEK293T cells were thus